Chaos
An Interdisciplinary Journal of Nonlinear Science

REVIEW ARTICLE | FEBRUARY 05 2024

# Order parameter dynamics in complex systems: From models to data FREE

Zhigang Zheng ; Can Xu ; Jingfang Fan ; Maoxin Liu; Xiaosong Chen



*Chaos* 34, 022101 (2024)
https://doi.org/10.1063/5.0180340

# Order parameter dynamics in complex systems: From models to data

Cite as: Chaos 34, 022101 (2024); doi: 10.1063/5.0180340
Submitted: 9 October 2023 · Accepted: 14 December 2023 ·
Published Online: 5 February 2024



Zhigang Zheng,[1,a)] Can Xu,[1] Jingfang Fan,[2] Maoxin Liu,[2] and Xiaosong Chen[2,b)]

## AFFILIATIONS

[1]Institute of Systems Science, Huaqiao University, Xiamen 361021, China and College of Information Science and Engineering, Huaqiao University, Xiamen 361021, China
[2]School of Systems Science, Beijing Normal University, Beijing 100875, China and Institute of Nonequilibrium Systems, Beijing Normal University, Beijing 100875, China

[a)]**Author to whom correspondence should be addressed:** zgzheng@hqu.edu.cn
[b)]xschen@bnu.edu.cn

## ABSTRACT

Collective ordering behaviors are typical macroscopic manifestations embedded in complex systems and can be ubiquitously observed across various physical backgrounds. Elements in complex systems may self-organize via mutual or external couplings to achieve diverse spatiotemporal coordinations. The order parameter, as a powerful quantity in describing the transition to collective states, may emerge spontaneously from large numbers of degrees of freedom through competitions. In this minireview, we extensively discussed the collective dynamics of complex systems from the viewpoint of order-parameter dynamics. A synergetic theory is adopted as the foundation of order-parameter dynamics, and it focuses on the self-organization and collective behaviors of complex systems. At the onset of macroscopic transitions, slow modes are distinguished from fast modes and act as order parameters, whose evolution can be established in terms of the slaving principle. We explore order-parameter dynamics in both model-based and data-based scenarios. For situations where microscopic dynamics modeling is available, as prototype examples, synchronization of coupled phase oscillators, chimera states, and neuron network dynamics are analytically studied, and the order-parameter dynamics is constructed in terms of reduction procedures such as the Ott–Antonsen ansatz, the Lorentz ansatz, and so on. For complicated systems highly challenging to be well modeled, we proposed the eigen-microstate approach (EMP) to reconstruct the macroscopic order-parameter dynamics, where the spatiotemporal evolution brought by big data can be well decomposed into eigenmodes, and the macroscopic collective behavior can be traced by Bose–Einstein condensation-like transitions and the emergence of dominant eigenmodes. The EMP is successfully applied to some typical examples, such as phase transitions in the Ising model, climate dynamics in earth systems, fluctuation patterns in stock markets, and collective motion in living systems.



**An order parameter is an important quantity measuring the symmetry breaking and the emergence of new orderings in complex systems. Traditionally, the order parameter is empirically introduced based on the understanding of specific physical backgrounds and the dynamics of complex systems. As a matter of fact, an order parameter should be a quantity embedded in state space, representing a part of degrees of freedom. Synergetic theory proposed the slaving principle with the physical language of the competitions between slow and fast degrees of freedom and the emergence of slow modes. This can be understood as a physics version of the central-manifold theorem and the adiabatic elimination method. Technically, the slaving principle provides a diagonalization procedure for identifying the slow mode. At the onset of a macroscopic transition, the slow mode becomes unstable and evolves to be the order parameter signifying the new collective ordering in complex systems. This idea has been extensively applied to various collective behaviors of complex systems. Recent years witnessed the storming explorations of large-scale data that are collected from various complex systems. One is faced with the challenge of disclosing intrinsic orderness and self-organization embedded complex data. The recently proposed eigen-microstate approach (EMA) has revealed these eigenmodes and transitions among these different macroscopic states. This approach actually offers a numerical way of identifying various modes and picking up the key order parameters at the onset of transitions.**

## I. INTRODUCTION

Understanding the intrinsic mechanism of collective behaviors of coupled units has become a focus for a variety of fields, such as biological neurons, circadian rhythm, chemically reacting cells, and even social systems.[1] Various collective dynamics, such as collective sustained oscillation in excitable networks, synchronization of coupled oscillators, swarming and flocking in active matters, and spatiotemporal pattern formations in nonlinear media, have been extensively observed. These behaviors manifest in different ways, but they share some common intrinsic mechanisms. Some properties of collective behaviors depend on the complexity of the system, while the other properties, such as phase transitions, may be the collaboration-induced emergence and can be described by low-dimensional dynamics with macroscopic variables.[2] Discovering the method to simplify the system is just as important and fascinating as the discovery of its complexity.

An order parameter is a key quantity in measuring the symmetry breaking and the emergence of new order in complex systems, which was first introduced to study phase transitions in thermodynamic systems with the aid of statistical physics.[3] This concept was thereafter extended to studies of non-equilibrium behaviors in complex systems, and the dynamical behaviors of order parameters found their more comprehensive applications in spatiotemporal behaviors in various systems ranging from physics and chemistry to biology and even social and economic systems.[4]

The emergence of ordered dynamics is the process of dimension reduction of the dynamical space of a complex system. Traditionally, one empirically "defines" or "constructs" an order parameter based on observations, experiences, or intuitions. It should be stressed that the existence of an order parameter is a natural and intrinsic feature for the emerging properties of complex systems. According to synergetic theory,[4] order parameters are intrinsically embedded in the state variables of complex systems as slow modes. The emergence of order parameters is the consequence of competitions between slow and fast modes. At the onset of critical points, the slow degrees of freedom embedded in the huge number of stable variables may become unstable and grow to emerge, which are determined by the center manifold theorem or the slaving principle.

Like most cases in physics, the simplification and low-dimensional reduction are associated with the symmetry property of the system. As the identity of gas particles is the foundation of statistical mechanics and collective variables as temperature and pressure, the identity of the coupled units in a complex system is also related to some order parameters.

Taking synchronization as an example, Winfree[5] and later Kuramoto[1] proposed simple versions of models as coupled phase oscillators with the mean-field coupling and gave an analytical self-consistency (SC) theory in the statistical sense. In 2008, Ott and Antonsen proposed the so-called Ott–Antonsen (OA) ansatz[6,7] by considering the competition of multiple parameters and the dependence of most of the parameters on some specific order parameters. This is a manifestation of the role of slaving principle. Similar dimension reduction idea can be applied to other issues, among which successful applications include the exploration of coherence–incoherence co-existed chimeras patterns,[8] collective dynamics of networks of neurons,[9] swarming dynamics of interacting active units[10] or even oscillators (swarmalators).[11]

Most complex systems in reality are so complicated that one often fails in accessing the intrinsic features based on a simple microscopic reconstruction modeling scenario. Nevertheless, modern techniques enable a vast and fast accumulation of big data. One can execute various experiments to obtain the data of a complex system. The new century of explorations of complexity is facing the situation of big data that are collected for various systems and situations. With the fast developments of computer and Internet, huge amounts of data have been accumulated in databases, and more and more data are continually produced on purposes in various fields of great diversity, such as neuron networks,[12] gene-regulating networks,[13] financial and business networks,[14] and so on. These data contain rich information of dynamical behaviors and intrinsic correlations embedded in complex systems. However, digging the dynamics and intrinsic structures of complex systems that generate these data is still a great challenge. Hence, a natural question is how to extract as much as possible information from these data.

Depicting dynamics and structures from available variable data are essentially an inverse problem, and it has become a fascinating task in various interdisciplinary fields. Different methods have been proposed to solve various inverse problems. The first successful testboard for revealing intrinsic information is the blossom of complex networks, which may infer rich topological information of interaction among units in complex systems.[15–20] In contrast to the progresses in complex networks, searching for intrinsic ordering of dynamical information still remains a great challenge.

Traditional analysis and mining of dynamical data are largely based on the computation of correlation and related quantities. Seeking for order parameters and their evolutions are big issues. Recently, an inspiring statistical approach called the *eigen-microstate approach* was proposed[21] in practically dealing with the extraction of order-parameter information from spatiotemporal data of complex systems. The focus of the eigen-microstate approach is various complex systems with distinctly different physical backgrounds. The common source from these different systems is the spatiotemporal data.

In this review, we endeavor to propose a framework that bridges the theoretical explorations with practical investigations of order-parameter dynamics in complex systems. The emergence of macroscopic orderness is the consequence of self-organization of the large number of microscopic degrees of freedom and the breaking of certain symmetries of complex systems. At the onset of the transition to ordered states, a few degrees of freedom act as slow modes and dominate the macroscopic evolution of the system. This procedure can be effectively treated based on the slaving principle of synergetic theory, which provides a powerful way of macroscopic reduction of complex systems starting from the microscopic level. We adopt the synchronization behavior of a population of oscillators as one example. The collective organization and the onset of synchronization can be studied analytically with the viewpoint of statistical physics. Based on the reduction procedures, such as the Ott–Antonsen ansatz, which is a variation of the central-manifold theorem, the order-parameter dynamics can be effectively derived.

A similar idea can be applied to the understanding of nonlinear dynamics of networks of neurons. Practically, the reduction idea of synergetics can be well facilitated in terms of the eigen-microstate approach when only spatiotemporal data instead of mathematical modeling in a complex system are available. This decomposition procedure intends to separate various eigenmodes from sophisticated data and measure the significance of these modes. This approach has proved to be very efficient and has been applied to various complex systems ranging from physics, earth dynamics, economics, and swarming dynamics.

This review is arranged as follows. In Sec. II, we give a brief introduction to the order-parameter theory by adopting basic ideas of the slaving principle in the core of synergetic theory, which describes the emerging process of order parameters. The mathematical formulation of this principle is proposed in the spirit of adiabatic elimination. By applying the slaving principle, the universal equations of motion governing order-parameter dynamics are discussed at the onset of Hopf instability and Turing instability, respectively. In Sec. III, as an application of the basic order-parameter theory, the statistical description of the synchronization dynamics of coupled phase oscillators is discussed.

In Sec. IV, as the application of order-parameter theory on synchronization of phase oscillators, we study the interesting chimera dynamics. In Sec. V, we adopt the quadratic integrate-and-fire (QIF) description of a single neuron, and the collective dynamics on networks can be dealt with by introducing the Lorentz ansatz. Macroscopically, the dynamics of the system can be described by the dynamics of the firing rate and the membrane voltage. We further discuss the recently proposed eigen-microstate approach to study the practical examples in Sec. VI. A summary is given in Sec. VII.

## II. SYNERGETIC PRINCIPLES FOR THE EMERGENCE OF ORDER PARAMETERS

As a preliminary step, we first focus on general principles for the reduction of dynamics in complex systems. It is important to seek for appropriate macroscopic variables that may reveal the emergence of macroscopic structures, and they act as order parameters similar to studies of those in-phase transitions.

Haken and collaborators proposed the synergetic theory and focused on the conditions, features, and evolution laws of the self-organization in a complex system with a large number of degrees of freedom under the drive of external parameters, and the interaction between subsystems to form spatial, temporal, or functional ordered structures on a macroscopic scale. The slaving principle as the core of synergetics, reveals how order parameters emerge from a large number of degrees of freedom through competitions and collaborations. As the system approaches the critical point, only a small number of modes/variables with a slow relaxation dominate the macroscopic behavior as order parameters of the system and characterize the global dynamics of the system. All those fast-relaxing modes are governed by the order parameters and can be adiabatically eliminated. The evolution of the low-dimensional equations of order parameters can be conveniently used to study the emergence of various non-equilibrium states, their stability, and bifurcations/transitions.

### A. Slaving principle and adiabatic elimination

Let us start from the simple two-dimensional nonlinear dynamical system with state variables $(u(t), s(t))$, whose evolution is governed by the following nonlinear differential equations:

$$\dot{u} = \alpha u - us, \tag{1a}$$

$$\dot{s} = -\beta s + u^2, \tag{1b}$$

where the coefficient $\beta > 0$, and $\alpha$ is the modulating parameter. The stationary solution $(u, s) = (0, 0)$ is stable for $\alpha < 0$. By modulating $\alpha$ from $\alpha > 0$ to $0 < \alpha \ll \beta$, the fixed-point solution $(u, s) = (0, 0)$ loses its stability by bifurcating to the new solution $(s, u) = (\alpha, \sqrt{\alpha\beta})$. Near the solution (0,0), $s(t)$ can be integrated from Eq. (1b) as

$$\begin{aligned} s(t) &= \int_0^t \exp[-\beta(t-\tau)]u^2(\tau)d\tau \\ &= \frac{1}{\beta}u^2(t) - \frac{2}{\beta}\int_0^t \exp[-\beta(t-\tau)u(\tau)\dot{u}(\tau)d\tau. \end{aligned} \tag{2}$$

For $0 < \alpha \ll \beta$, a scaling estimation leads to the main scaling dependence as $u \sim \alpha^{1/2}, s \sim \alpha, \dot{u} \sim \alpha^{3/2}$, and $\dot{s} \sim u\dot{u} \sim \alpha^2$. One, thus, obtains $s(t) \approx u^2(t)/\beta$ in (2) by discarding higher-order term. In fact, $\dot{s} \sim \alpha^2$ also indicates that one may set $\dot{s} = 0$ in Eq. (1b) and get $s(t) = u^2(t)/\beta$. Substituting this expression to Eq. (1a), one obtains the following one-dimensional dynamical equation:

$$\dot{u} = \alpha u - \frac{1}{\beta}u^3. \tag{3}$$

This procedure is the essence of the *adiabatic elimination principle*, indicating that $u(t)$ is the slow mode, and $s(t)$ is the fast mode. Near the onset of bifurcation $0 < \alpha \ll \beta$, the fast mode $s(t)$ can always keep up with the change of the slow mode as the function of the slow variable, $u(t)$, i.e., the slow mode dominates the evolution of the system. Therefore, the slow mode $u(t)$ can be identified as the order parameter, which is described by the one-dimensional equation (3).

For higher-dimensional systems, suppose an $n$-dimensional dynamical system $\dot{\boldsymbol{x}} = \boldsymbol{F}(\alpha, \boldsymbol{x})$ with $\alpha$ being the controlling parameter set, and $\boldsymbol{x} = (x_1, x_2, \ldots, x_n)^T$ is an $n$-dimensional state vector. The equations of motion can be written in canonical form near the fixed point $\boldsymbol{x} = 0$ as

$$\dot{\boldsymbol{x}} = \mathbf{A}(\alpha)\boldsymbol{x} + \boldsymbol{B}(\alpha, \boldsymbol{x}), \tag{4}$$

where $\mathbf{A} = \mathbf{A}(\alpha)$ is an $n \times n$ Jacobian matrix and $\boldsymbol{B}(\alpha, \boldsymbol{x})$ is an $n$-dimensional nonlinear function vector of $\boldsymbol{x}$. The eigenvalues of the matrix $\mathbf{A}$ are $\{\lambda_i(\alpha)\}$, which are aligned as the descending order according to their real parts, $\mathrm{Re}\lambda_1 \geq \mathrm{Re}\lambda_2 \geq \cdots \geq \mathrm{Re}\lambda_n$.

The solution $\boldsymbol{x} = 0$ is assumed to be stable in a certain parameter regime of $\alpha$, i.e., the real parts of all eigenvalues are negative, $\mathrm{Re}\lambda_i(\alpha) < 0, i = 1, 2, \ldots, n$. By modulating $\alpha$ above the critical value, i.e., $\alpha > \alpha_c$, $0 < \mathrm{Re}\lambda_1 \ll 1$ and $\mathrm{Re}\lambda_i < 0$ for $i \geq 2$, the solution $\boldsymbol{x} = 0$ becomes unstable. The Jacobian $\mathbf{A}$ can be diagonalized by

introducing the linear transformation matrix $\mathbf{T}$ as

$$\tilde{\mathbf{A}} = \mathbf{T}^{-1}\mathbf{A}\mathbf{T} = \begin{bmatrix} \lambda_1 & 0 & 0 & \cdots & 0 \\ 0 & \lambda_2 & 0 & \cdots & 0 \\ \cdots & \cdots & \cdots & \cdots & \\ 0 & \cdots & 0 & 0 & \lambda_n \end{bmatrix}. \tag{5}$$

We relabel these eigenvalues by separating them into two groups, one group is composed of $1 \le m \ll n$ eigenvalues with the same largest real part $\left\{\lambda_u^{i=1,\ldots,m}\right\} = \{\lambda_1, \ldots, \lambda_m\}$, the other group is composed of the rest $n-m$ eigenvalues as $\left\{\lambda_s^{i=1,\ldots,n-m}\right\} = \{\lambda_{n-m+1}, \ldots, \lambda_n\}$, where $Re\lambda_s^i < 0, i = 1, 2, \ldots, n-m$. Then, the corresponding state vector $\boldsymbol{x}$ can be decomposed into sub-vectors as

$$(\boldsymbol{u}, \boldsymbol{s})^T = \mathbf{T}\boldsymbol{x}. \tag{6}$$

Equation (4) can be rewritten as

$$\dot{\boldsymbol{u}} = \lambda_u \boldsymbol{u} + \tilde{B}_u(\boldsymbol{u}, \boldsymbol{s}), \tag{7a}$$

$$\dot{\boldsymbol{s}} = -\lambda_s \boldsymbol{s} + \tilde{\boldsymbol{B}}_u(\boldsymbol{u}, \boldsymbol{s}), \tag{7b}$$

where the slow-varying manifold $\boldsymbol{u} = (u_1, u_2, \ldots, u_m)^T$, and the fast manifold $\boldsymbol{s} = (s_1, s_2, \ldots, s_{n-m})^T$. $\tilde{\boldsymbol{B}}_u = \left(\tilde{B}_u^1, \tilde{B}_u^2, \ldots, \tilde{B}_u^m\right)^T$ and $\tilde{\boldsymbol{B}}_s = \left(\tilde{B}_s^1, \tilde{B}_s^2, \ldots, \tilde{B}_s^{n-m}\right)^T$ are the nonlinear terms.

Therefore, one successfully separates the slow modes $\boldsymbol{u}(t)$ from all the variables in terms of the transformation (7a), and the remaining variables $\boldsymbol{s}_i(t), i = 1, 2, \ldots, n-1$ are fast modes that satisfy Eq. (7b). The adiabatic elimination procedure can be applied to (7b) by setting $\dot{\boldsymbol{s}} = 0$, leading to the following $n-m$ equations:

$$\lambda_s \boldsymbol{s} = -\tilde{\boldsymbol{B}}_s(\boldsymbol{u}, \boldsymbol{s}). \tag{8}$$

Fast variables $\boldsymbol{s}$ can then be analytically solved from the $n-m$ equations of (8) as the function of the slow variable $\boldsymbol{u}$ in the form of $\boldsymbol{s} = \boldsymbol{s}(\boldsymbol{u})$. Then, by inserting $\boldsymbol{s}(\boldsymbol{u})$ into Eq. (7a), one obtains

$$\dot{\boldsymbol{u}} = \lambda_u \boldsymbol{u} + \tilde{B}_u(\boldsymbol{u}, \boldsymbol{s}(\boldsymbol{u})). \tag{9}$$

These $m$ equations describe the evolution of the order parameters $\boldsymbol{u} = (u_1, u_2, \ldots, u_m)^T$. Generally, the dynamical dimension of the order-parameter space $m \ll n$.

Equation (9) has the same form as Eq. (7), but they are essentially different. In Eq. (7), $\mathbf{s} = \mathbf{s}(t)$, while in Eq. (9), $\mathbf{s} = \mathbf{s}(\mathbf{u})$, implying that fast variables are functions of the slow variables. The degrees of freedom of (9) is considerably less than that of (7). In practice, only a very small portion of modes may lose their stability at the critical point; therefore, one can consider the procedure from Eqs. (4) to (7) and (9) as a reduction from high-dimensional to low-dimensional dynamics governed by only a few order parameters. This is a great dynamical simplification, which is an important contribution of the slaving principle at the critical point.

### B. Spatiotemporal dynamics: The Ginzburg–Landau paradigm

The above synergetic principle can be well applied to studies on the formation of spatial or temporal orderings as long as the dynamics of the principal order parameters are derived. A prototype modeling of a spatiotemporal pattern dynamics is the reaction–diffusion system, which is mathematically described by the following partial differential equation:

$$\partial_t \boldsymbol{C} = \boldsymbol{f}(\boldsymbol{C}, \mu) + \mathbf{D}\nabla^2 \boldsymbol{C}, \tag{10}$$

where $\boldsymbol{C} = \boldsymbol{C}(\boldsymbol{r}, t)$ is the state vector, $\mu$ is the set of control parameters, $\boldsymbol{f}$ represents the nonlinear dynamics function vector, $\nabla = \partial^2/\partial \boldsymbol{r}^2$ is the Laplacian operator, and $\mathbf{D}$ is the diffusion coefficient tensor. Different boundary conditions and initial conditions should be considered to solve Eq. (10).

Suppose the system possesses a spatially homogeneous ($\mathbf{D}\nabla^2\boldsymbol{C} = 0$) and temporarily stationary ($\partial_t \boldsymbol{C} = 0$) solution $\boldsymbol{C}(\boldsymbol{r}, t) = \boldsymbol{C}_0$, which can be easily derived from (10) by setting $\boldsymbol{f}(\boldsymbol{C}, \mu) = 0$. Linear stability analysis can be performed to this solution. We further assume that there exists a critical point $\mu = \mu_c$, below which the stationary state is stable while unstable when $\mu > \mu_c$. For the simplest case, the state vector for $\mu \ge \mu_c$ can be decomposed into

$$\boldsymbol{C}(\boldsymbol{r}, t) = \boldsymbol{C}_0 + \sum_{i=1}^{N} \left[A_i(\boldsymbol{r}, t) e^{\mathrm{i}(\boldsymbol{k}\cdot\boldsymbol{r} + \omega_i t)} + c.c.\right], \tag{11}$$

where $\{A_i\}$ are complex amplitudes of different spatiotemporal modes $\{\boldsymbol{k}_i, \omega_i\}$.

By considering the loss of stability at $\mu > \mu_c$, for the spatial and temporal modes, respectively, a saddle-node instability may occur for $\omega = 0$, while a Hopf instability satisfies $\boldsymbol{k} = 0$.

Let us discuss these two cases:

$$\partial_t A_i = s_i A_i + F_i\left(A_i, \left\{A_{j\neq i}\right\}\right). \tag{12}$$

In Eq. (12), function $F_i$ describes the coupling between the $i$th normal mode and other modes $\left\{A_{j\neq i}\right\}$. $\{s_i\}$ represent the eigenvalue coefficients, which describes the growth rate of the modes $\{A_i\}$. These modes can be classified two types according to the sign of $\mathrm{Re}s_i$:

(1) $\mathrm{Re}s_i < 0$: This corresponds to a linearly diverging mode. Only a very few modes, say, one or two modes may lose their stability at the critical point. These several modes are obviously slow modes in terms of the slaving principle discussed above. We also call them *active modes*.
(2) $\mathrm{Re}s_i > 0$: These modes are identified as slave or slow modes and can be adiabatically eliminated according to synergetic principles or the center manifold theorem.

Therefore, one has $\{A_i\} = \left\{A_s, A_f\right\}$. Equation (12) can be rewritten as the following two groups of equations:

$$\partial_t A_{s,f} = f_{s,f}(A_s, A_f). \tag{13}$$

Near the critical point, the slaving principle enables one to eliminate fast modes $A_f$. By setting $\partial_t A_f = f_f(A_s, A_f) = 0$, one works out $A_f = g(A_s)$. Therefore, Eq. (13) is reduced to

$$\partial_t A_s = f_s(A_s, g(A_s)) = F(A_s). \tag{14}$$

In the following discussions, we omit the subscript "s," and all modes are slow normal modes. These complex modes $\{A_i\}$ satisfy

$$\partial_t A_i = F_i\left(A_i, \bar{A}_i, \left\{A_{j\neq i}, \bar{A}_{j\neq i}\right\}\right). \tag{15}$$

### 1. Turing instability

The Turing instability implies the spatial inhomogeneity when $\mu > \mu_c$. An ideal Turing pattern is composed of $N$ wave-vector pairs $\{\boldsymbol{k}_i, -\boldsymbol{k}_i; i = 1, 2, \ldots, N\}$ as a linear combination:

$$C(\boldsymbol{r}) = C_0 + \sum_{i=1}^{N} \left(A_i e^{\mathrm{i}\boldsymbol{k}\cdot\boldsymbol{r}} + c.c.\right), \tag{16}$$

where $A_i$ are complex normal modes satisfying Eq. (15).

For the spatially one-dimensional case, only $N = 1$ normal mode is relevant, and Eq. (15) becomes

$$\partial_t A(x) = F\left(A(x), \bar{A}(x)\right). \tag{17}$$

In the vicinity of the critical point $\mu_c$, function $F$ can be expanded around $A = 0$ in terms of the Taylor series. In the third order, one has

$$\begin{aligned}\partial_t A = {} & a_1^1 A + a_1^2 \bar{A} + a_2^1 A^2 + a_2^2 A\bar{A} + a_2^3 \bar{A}^2 + a_3^1 A^3 + a_3^2 A^2 \bar{A} \\ & + a_3^3 A\bar{A}^2 + a_3^4 \bar{A}^3 + O\left(A^4\right).\end{aligned} \tag{18}$$

The symmetries of the system require that Eq. (18) is invariant under the translational transformation $x \to x + x_0$ [equivalently $A(x) \to A(x)e^{\mathrm{i}\varphi}$] and the mirror transformation $x \to -x$ [equivalently $A(x) \to \bar{A}(x)$], leading to only $a_1^1$ and $a_3^2$ in Eq. (18) non-zero. By setting $a_1^1 = 1$ and $a_3^2 = -c$, one gets

$$\partial_t A = A - c\,|A|^2 A. \tag{19}$$

This one-dimensional amplitude equation is the normal form of the order-parameter equation.

For spatially two- or three-dimensional cases, the spatially rotational invariance requires the participation of more normal modes in constructing the pattern formation. Based on the Taylor expansion at $\mu \geq \mu_c$ to the third order, the amplitude equation can be expressed as

$$\partial_t A_k = \mu A_k + \sum_{l,m} a_{lm} A_l A_m + \sum_{l,m,n} b_{lmn} A_l A_m A_n + O\left(A^4\right). \tag{20}$$

The translational invariance, i.e., the invariance of Eq. (20) under $A_k \to A_k e^{\mathrm{i}\boldsymbol{k}_k\cdot\boldsymbol{r}_0}$, gives rise to the following *spatial resonance conditions*:

$$\begin{aligned}&\textbf{Second order: } \boldsymbol{k}_l + \boldsymbol{k}_m = \boldsymbol{k}_k, \\ &\textbf{Third order: } \boldsymbol{k}_l + \boldsymbol{k}_m + \boldsymbol{k}_n = \boldsymbol{k}_k,\end{aligned} \tag{21}$$

where $\boldsymbol{k}_l, \boldsymbol{k}_m, \boldsymbol{k}_n, \boldsymbol{k}_k, \ldots$ are the wave vectors corresponding to the normal modes $A_l, A_m, A_n, A_k, \ldots$, respectively. Moreover, $|\boldsymbol{k}_l| = |\boldsymbol{k}_m| = |\boldsymbol{k}_n| = |\boldsymbol{k}_k|$. The spatial resonance condition reduces the amplitude equation to

$$\partial_t A_i = \mu A_i + a\bar{A}_j \bar{A}_k - \left[b_1 |A_i|^2 + b_2\left(|A_j|^2 + |A_k|^2\right)\right] A_i, \tag{22}$$

where $i, j, k = 1, 2, 3$, and $i \neq j \neq k$. All coefficients in Eq. (22) are real due to the mirror symmetry. Equation (22) is the order-parameter equation for the analysis of two-dimensional Turing-pattern formation in general systems.

### 2. Hopf instability

Let us briefly discuss the temporal structure formation at the onset of Hopf instability related to a temporal instability of the stationary solution. For the single-mode case, this corresponds to the state vector,

$$C(t) = C_0 + A(\tau)e^{\mathrm{i}\omega t} + c.c., \tag{23}$$

where $\tau$ describes the time scale of the slow mode, and $\omega$ is the characteristic frequency at the onset of instability, and the *c.c.* means the complex conjugate. The eigenvalues $a_1^1 = \lambda + \mathrm{i}\omega$, and the amplitude equation can be similarly written in the form of Fourier expansion,

$$\begin{aligned}dA/d\tau = {} & (\lambda + i\omega)A + a_1^2 \bar{A} + a_2^1 A^2 + a_2^2 A\bar{A} + a_2^3 \bar{A}^2 \\ & + a_3^1 A^3 + a_3^2 A^2 \bar{A} + a_3^3 A\bar{A}^2 + a_3^4 \bar{A}^3 + O\left(A^4\right).\end{aligned} \tag{24}$$

The translational invariance under $A \to Ae^{\mathrm{i}\varphi}$ implies naturally that only coefficients $a_1^1 = \lambda + \mathrm{i}\omega$ and $a_3^2$ are non-zero. To the third order, $a_3^2 < 0$. Denoting $a_3^2 = -c$ and $\tau \to t$, Eq. (24) is reduced to the Stuart–Landau equation

$$dA/dt = (\lambda + \mathrm{i}\omega)A - c\,|A|^2 A. \tag{25}$$

Equation (25) describes the limit-cycle motion of the solution form $A(t) = re^{\mathrm{i}\omega t}$ with the radius $r = \sqrt{\lambda/c}$ and the frequency $\omega$. For a complex $c$, Eq. (25) can be generalized to

$$dA/dt = (\lambda + \mathrm{i}\omega)A - (c_1 + \mathrm{i}c_2)\,|A|^2 A. \tag{26}$$

By further considering the spatial diffusion effect, the amplitude equation can be written as the following complex Ginzburg–Landau equation (CGLE):

$$\partial_t A(\boldsymbol{r}, t) = (\lambda + \mathrm{i}\omega)A - (c_1 + \mathrm{i}c_2)\,|A|^2 A + (D_1 + \mathrm{i}D_2)\nabla^2 A. \tag{27}$$

CGLE has been extensively studied in relation to spatiotemporal dynamics.[22–25]

## III. SYNCHRONIZATION: ORDER-PARAMETER REDUCTION SCHEMES

Phase description of limit-cycle motion is a reduction of oscillation by neglecting the amplitude effect. Winfree for the first time proposed the phase modeling of coupled oscillators and found the synchronization transition when the oscillators have narrow deviations of natural frequencies.

Kuramoto probably proposed the first statistically tractable mean-field model to investigate the synchronization transition. The Kuramoto model consists of a population of $N$ coupled phase oscillators $\{\theta_i(t)\}$ with natural frequencies $\{\omega_i\}$ with the distribution $g(\omega)$. A single oscillator can be simply described by $\dot{\theta}_i = \omega_i$. By considering a general network connection topology, the dynamics of $N$ interacting oscillators are governed by

$$\dot{\theta}_i = \omega_i + \frac{K}{d_i + 1} \sum_{j=1}^{N} A_{ij} \sin(\theta_j - \theta_i),\ i = 1, \ldots, N. \tag{28}$$

Here, $K$ is the coupling strength and $d_i$ denotes the degree, i.e., the number of neighbors of the $i$th oscillator. $\mathbf{A} = \left(A_{ij}\right)$ is the adjacency matrix indicating the connections among oscillators, and $A_{ij} = 1$

implies a non-zero interaction between the $i$th and $j$th oscillators, whereas $A_{ij} = 0$ means no interaction between two elements.

For the traditional Kuramoto model, global coupling, i.e., $A_{ij} = 1$ is adopted, and $d_i = N - 1$. Then, the equations of motion is written as

$$\dot{\theta}_i = \omega_i + \frac{K}{N}\sum_{j=1}^{N}\sin(\theta_j - \theta_i), \quad i = 1, \ldots, N. \tag{29}$$

One may introduce a coherence factor as

$$\alpha = \frac{1}{N}\sum_{j=1}^{N} e^{\mathrm{i}\theta_j}. \tag{30}$$

In the limit $N \to \infty$, $|\alpha| = 0$ represents an incoherent state with phases of oscillators homogeneously distributed in $[0, 2\pi)$. $|\alpha| > 0$ implies some degree of synchrony among oscillators, and $|\alpha| = 1$ means a fully in-phase synchronous state. Kuramoto proposed the SC approach and analytically obtained the synchronization transition at the critical coupling $K_c = 2/[\pi g(0)]$.

By using (30), Eq. (29) can be rewritten as

$$\dot{\theta}_i = \omega_i + \frac{K}{2\mathrm{i}}\left(\alpha e^{-\mathrm{i}\theta_i} - \bar{\alpha} e^{\mathrm{i}\theta_i}\right), \quad i = 1, \ldots, N, \tag{31}$$

where $\bar{\alpha}$ is the complex conjugate of $\alpha$. An important feature as shown in Eq. (31) that the mean-field factor $\alpha$ governs the dynamics of each oscillator in the system, which can be adopted as the order parameter to describe the macrostate of the system.

A more general form of the mean-field model with phase oscillators can be written as

$$\dot{\theta}_i = F(\boldsymbol{\alpha}, \theta_i, \boldsymbol{\beta}, \boldsymbol{\gamma_i}), \quad i = 1, \ldots, N, \tag{32}$$

where $F(\boldsymbol{\alpha}, \theta_i, \boldsymbol{\beta}, \boldsymbol{\gamma_j})$ is a smooth, real, $2\pi$-periodic function of the phase variable $\theta_i$. $\boldsymbol{\alpha} = (\ldots, \alpha_{-1}, \alpha_0, \alpha_1, \ldots)$ is a generalized order-parameter set with the $n$th order parameter $\alpha_n$ defined as

$$\alpha_n = \frac{1}{N}\sum_{j=1}^{N} e^{\mathrm{i}n\theta_j}. \tag{33}$$

Obviously, the component $\alpha_1$ is just the factor $\alpha$ defined by (30). In (32), $\boldsymbol{\beta} = (\beta_1, \beta_2 \cdots \beta_s)$ is the homogeneous-parameter set, whose elements are identical for all oscillators, e.g., the coupling strength $K$. $\boldsymbol{\gamma_i} = \left(\gamma_i^{(1)}, \gamma_i^{(2)}, \ldots, \gamma_i^{(l)}\right)$ represents the heterogeneous-parameter set, for example, the natural frequency $\{\omega_j\}$, whose elements are non-identical for different oscillators and are usually assumed to obey the statistical distribution $g(\omega)$.

### A. Reduction paradigm for coupled identical oscillators

We first consider a set of identical oscillators, e.g., $\gamma_i = \omega_i = \omega^*, i = 1, 2, \ldots, N$. The equations of motion read

$$\dot{\theta}_i = F(\boldsymbol{\alpha}, \theta_i, \boldsymbol{\beta}), \quad i = 1, \ldots, N. \tag{34}$$

In thermodynamic limit $N \to \infty$, the statistical description of this system can be adopted, i.e., the distribution function of the phase $\rho_\gamma(\theta, t)$ can be introduced, and $\rho_\gamma(\theta, t)d\theta$ denotes the fraction of oscillators with the phase lying between $\theta$ and $\theta + d\theta$. Because each oscillator in Eq. (34) moves with an angular velocity $v = F(\boldsymbol{\alpha}, \theta, \boldsymbol{\beta})$, the density $\rho_\gamma(\theta, t)$ obeys the continuity equation,

$$\frac{\partial \rho_\gamma}{\partial t} + \frac{\partial(\rho_\gamma v)}{\partial \theta} = 0. \tag{35}$$

The complex order parameters $\alpha_n$ can be expressed as the $n$th momentum of $e^{\mathrm{i}\theta}$,

$$\alpha_n = \int_0^{2\pi} \rho_\gamma(\theta, t) e^{\mathrm{i}n\theta} d\theta, \quad n = 1, 2, \ldots. \tag{36}$$

It is important to study the evolution equation of order parameters $\alpha_n$. By performing the time derivative of both sides of Eq. (36) and using the continuity equation (35), after the partial integral of the right-hand part, the evolution of order parameters $\alpha_n$ can be obtained as

$$\dot{\alpha}_n = \int_0^{2\pi} e^{\mathrm{i}n\theta}\frac{\partial \rho_\gamma(\theta, t)}{\partial t} d\theta = \mathrm{i}n\int_0^{2\pi} e^{\mathrm{i}n\theta} F(\boldsymbol{\alpha}, \theta, \boldsymbol{\beta})\rho_\gamma(\theta, t) d\theta. \tag{37}$$

Because the coupling function $F(\boldsymbol{\alpha}, \theta, \boldsymbol{\beta})$ is always $2\pi$-periodic for $\theta$, one can introduce the Fourier expansion of $F(\boldsymbol{\alpha}, \theta, \boldsymbol{\beta})$,

$$F(\boldsymbol{\alpha}, \theta, \boldsymbol{\beta}) = \sum_{j=-\infty}^{\infty} f_j(\boldsymbol{\alpha}, \boldsymbol{\beta}) e^{\mathrm{i}j\theta}. \tag{38}$$

Substituting the Fourier expansion (38) into these equations, one obtains

$$\dot{\alpha}_n = \mathrm{i}n\sum_{j=-\infty}^{\infty} f_j(\boldsymbol{\alpha}, \boldsymbol{\beta})\alpha_{j+n}. \tag{39}$$

For the simplest case,

$$F(\boldsymbol{\alpha}, \theta) = f_1(\boldsymbol{\alpha}) e^{\mathrm{i}\theta} + \bar{f}_1(\boldsymbol{\alpha}) e^{-\mathrm{i}\theta} + f_0(\boldsymbol{\alpha}). \tag{40}$$

Equation (39) becomes

$$\dot{\alpha}_n = \mathrm{i}n\left(f_1\alpha_{n+1} + \bar{f}_1\alpha_{n-1} + f_0\alpha_n\right), \tag{41}$$

where $n \geq 0$ and $\alpha_{-n} = \bar{\alpha}_n$. This is a set of tridiagonal recursion equations, and the solution of these equations can be obtained for some specific cases.

In fact, extensive studies revealed low-dimensional dynamical properties when oscillators are in the synchronized state at strong couplings. Synchronization bifurcation-tree cascades of coupled phase oscillators imply the microscopic self-organization and the reducibility of the coupled phase oscillator systems.[26–29] Low-dimensional property of order-parameter dynamics is the natural consequence of synergetic theory and indicates that order parameters $\{\alpha_n\}$ are related to each other. We may suppose the simplest case $\alpha_n = F(\alpha_1, n)$, a strict deduction[30,31] can lead to the Ott–Antonsen (OA) ansatz,[6,7]

$$\alpha_n = F(\alpha_1, n) = \alpha_1^n. \tag{42}$$

Therefore, all the equations for $\alpha_n$ are reduced to

$$\dot{\alpha}_1 = \mathrm{i}\left[f_1(\alpha_1)\alpha_1^2 + \bar{f}_1(\alpha_1) + f_0(\alpha_1)\alpha_1\right]. \tag{43}$$

The OA ansatz also implies the existence of an invariant manifold, and the corresponding phase density defined on this manifold

is called the Poisson kernel distribution. In fact, the distribution function $\rho_\gamma(\theta,t)$ can be expanded according to the Fourier series with components being the order parameters $\alpha_n$,

$$\rho_\gamma(\theta,t)=\frac{1}{2\pi}\left\{1+\sum_{n=1}^{\infty}\left[\alpha_n(t)e^{-in\theta}+\bar{\alpha}_n(t)e^{in\theta}\right]\right\}. \tag{44}$$

By considering the OA ansatz (42), series (44) becomes a geometric progression and can be well worked out. The distribution function is finally expressed as

$$\rho_\gamma(\theta,t)=\frac{1}{2\pi}\frac{1-r^2}{1-2r\cos(\theta-\phi)+r^2}, \tag{45}$$

where $\alpha_1=re^{i\phi}$. Formula (45) indicates that the phase distribution is completely determined by $\alpha_1(t)$. The order parameter $\alpha_1(t)$ may vary with time, and this consequently leads to the change of the distribution $\rho_\gamma(\theta,t)$ with the evolution of the system. However, it can be easily found from (45) that $\rho_\gamma(\theta,t)$ always keeps an invariant form of the Poisson summation. If one starts from the Poisson-summation distribution $\rho_\gamma(\theta,t=0)$, the density distribution $\rho_\gamma(\theta,t)$ will keep invariant.

### B. Order-parameter dynamics of ensembles of nonidentical oscillators

Let us consider the case of nonidentical oscillators with different natural frequencies obeying the distribution $g(\omega)$. The above order-parameter analysis can be extended to general cases of nonidentical oscillators.

In the thermodynamic limit, one may introduce the density function $\rho(\omega,\theta,t)$, where $\rho(\omega,\theta,t)d\omega d\theta$ denotes the fraction of oscillators with the natural frequency and phase lying $\omega\to\omega+d\omega$ and $\theta\to\theta+d\theta$, respectively. The distribution density obeys the continuity equation

$$\frac{\partial\rho(\omega,\theta,t)}{\partial t}+\frac{\partial(v\rho(\omega,\theta,t))}{\partial\theta}=0, \tag{46}$$

where $v=F(\boldsymbol{\alpha},\theta,\boldsymbol{\beta},\omega)$. For oscillators with natural frequency $\omega\to\omega+d\omega$, the partial order parameters can be rewritten in terms of the statistical average of the factor $e^{i\theta}$ as

$$\alpha_n(\omega,t)=\int e^{in\theta}\rho(\omega,\theta,t)d\theta. \tag{47}$$

Then, the global order parameter for all oscillators with various natural frequencies is expressed as

$$\alpha_n(t)=\int\alpha_n(\omega,t)g(\omega)d\omega=\int\int e^{in\theta}\rho(\omega,\theta,t)d\omega d\theta. \tag{48}$$

The order parameter can also be understood as the $n$-order Fourier expansion of $\rho(\omega,\theta,t)$. The following recursive equation can be obtained using the continuity equation:

$$\dot{\alpha}_n(\omega,t)=in\sum_{j=-\infty}^{\infty}f_j(\boldsymbol{\alpha},\boldsymbol{\beta},\omega)\alpha_{j+n}(\omega,t). \tag{49}$$

If the coupling function contains only the first-order Fourier coefficients,

$$F(\boldsymbol{\alpha},\boldsymbol{\beta},\omega,\theta)=f_1e^{i\theta}+\bar{f}_1e^{-i\theta}+f_0, \tag{50}$$

then the Ott–Antonsen ansatz for a given frequency $\omega$,

$$\alpha_n(\omega,t)=\alpha_1^n(\omega,t), \tag{51}$$

is a set of special solutions of the order-parameter equations. Then, the equations of order parameters are reduced to

$$\dot{\alpha}_1(\omega,t)=i\left[f_1\alpha_1^2+\bar{f}_1+f_0\alpha_1\right]. \tag{52}$$

By using (48) for $n=1$, one can further obtain the equation of motion of the order parameter $\alpha_1(t)$ by integrating over $\omega$ for a given $g(\omega)$.

### C. Order-parameter dynamics of the traditional Kuramoto model

Let us adopt the traditional Kuramoto model described by Eq. (29) as an example to derive the governing equation of the order parameter.

One first denotes

$$z(t)=\frac{1}{N}\sum_{j=1}^{N}e^{i\theta}=\int\alpha_1(\omega,t)g(\omega)d\omega, \tag{53}$$

then Eq. (29) can be rewritten as the norm form

$$\dot{\theta}_i=\frac{Kz}{2i}e^{-i\theta_i}+\omega_i-\frac{Kz}{2i}e^{i\theta_i}, \tag{54}$$

where the coefficients corresponding to Eq. (52) are

$$f_1=-\frac{Kz}{2i},\quad \bar{f}_1=f_{-1}=\frac{Kz}{2i},\qquad f_0=\omega. \tag{55}$$

For the case of a Lorentzian distribution of the natural frequencies $g(\omega)=1/[\pi(\omega^2+1)]$, the integral (53) can be written as

$$z(t)=\int_{-\infty}^{\infty}\frac{\alpha_1(\omega,t)d\omega}{\pi(\omega^2+1)}. \tag{56}$$

The above integral can be analytically extended to the upper complex plane $\omega+i\delta$. In terms of the residue theorem, one can get $(t)=\alpha_1(\omega=i,t)$. Then, by inserting $\omega=i$ into Eq. (52), one easily gets the dynamical equation of the order parameter $z(t)$,

$$\dot{z}=\frac{1}{2}z\left(K-2-K|z|^2\right). \tag{57}$$

Therefore, the collective dynamics of the Kuramoto model can be conveniently analyzed in terms of the order-parameter dynamics. Equation (57) has two fixed point solutions: $z=0$, representing the incoherent state that oscillators move incoherently, and $|z|=\sqrt{(K-2)/K}$ implying a coherent motion, which exists only as $K\geq 2$. The transition from the incoherent state to the synchronized state occurs at the critical coupling $K\geq K_c=2$. This result agrees well with the traditional analysis in terms of the SC equation approach.[1]

### D. Some recent advances on synchronization dynamics

Synchronization is a fundamental topic in studies of collective behaviors of complex systems. There have been extensive explorations on this subject in terms of coupled phase oscillators. Here,

we list some representative studies according to the foundations on order-parameter theory and several typical applications.

### 1. Order-parameter dynamics: Theoretical framework construction

There have been great advances in the theoretical study of synchronization of coupled oscillators since the works of Winfree and Kuramoto. The *self-consistency (SC) method*,[1] to our knowledge, was the first successful and tractable scheme in the analytical treatment of synchronization transitions in terms of statistical approach. Mirollo and Strogatz further proposed the spectrum analysis on the stability of the synchronous and incoherent states.[32,33]

It has been found that coupled phase oscillators may exhibit very rich collective and even unsteady dynamics apart from the stationary synchronous solution. It is crucial to propose an insightful understanding of these dynamical coordinations. More reduction approaches have been proposed in recent two decades to deal with the low-dimensional reduction of the high-dimensional dynamics of coupled oscillators. Ott and Antonsen proposed the *OA ansatz*,[6,7] which is thought to be a breakthrough in grasping the essence of synchronization.

It is very interesting that in the early years, Watanabe and Strogatz found that a globally coupled oscillator system can be transformed into a three-dimensional dynamical system by introducing the complex Mobius transformation, which is thereafter called the *Watanabe–Strogatz transformation*.[34,35] The Ott–Antonsen ansatz and its consequence of the invariant Poisson kernel distribution are closely related to the Watanabe–Strogatz transformation. Marvel *et al.* showed that the group of Mobius transformations can be well applied to understand the collective synchrony of coupled phase oscillator systems.[36,37]

An interesting approach to accomplishing the dimension reduction in terms of order-parameter analysis is to find an approximate parametrization of the synchronization manifold by means of appropriately chosen collective coordinates. A *collective-coordinate reduction scheme* was proposed.[38–40] In this approach, an $N$-dimensional Kuramoto model is reduced to the $n$-dimensional dynamics with $n \ll N$. It was shown that the onset of both local and global synchronization is well reproduced with good numerical accuracy.

Very recently, the *Cestnik–Pikovsky ansatz* was proposed in probing more interesting collective dynamics in coupled phase oscillators.[41] This ansatz extends the OA approach by constructing a hierarchy of global exact finite-dimensional reductions, which includes the OA manifold as the zero-order case. In this approach, the chaotic collective dynamics, which are impossible within the OA manifold, are straightforwardly recovered.

### 2. Order-parameter dynamics: Applications

A large portion of efforts have been focused on the generalization of the paradigmatic Kuramoto model by considering various extensions that are related to different practical physical backgrounds. We will not discuss those variations for the Kuramoto discussed before 2005, interested readers may refer to the review article of Acebrón and co-authors.[42] Moreover, we will not either extend our discussions to Kuramoto on complex networks, which had been extensively summarized in the review.[43] The central extension of most of the studies has been concentrated to the couplings among oscillators. Below, we only list the progress on the following several topics in recent years.

*a. Frustration and contrarian-conformist competition.* Order-parameter theory has been applied to the study of coupled oscillators with more complicated competitions. Hong and Strogatz[44] considered a generalization of the Kuramoto model of oscillators with positively coupled conformists and negatively coupled contrarians. This model is simple and exactly solvable while exhibiting numerous interesting stationary and non-stationary collective states. The contrarian-conformist competition has recently been a focus of interest in coupled oscillators, which may induce numerous interesting behaviors.[45–53]

*b. Beyond the pairwise interaction.* Pairwise interaction is usually adopted as the standard paradigm of interactions in complex systems. In some cases, many-body interaction is important and can be observed in physical systems, social and economic systems, and neuronal networks. The impact of non-pairwise coupling on synchrony received much interest in recent years.[54–58] Such studies are usually performed as hypernetworks, simplicial complexes, many-body interactions, and high-order couplings.

Tanaka and Aoyagi first studied numerically and theoretically a system of phase oscillators with a three-body interaction and found infinite numbers of multistable synchronized states above a critical coupling strength.[54] Skardal *et al.*[55] and Xu *et al.*[57] studied the collective synchrony in systems of coupled phase oscillators with higher-order coupling. We investigated the extensive multicluster states induced by high-order structures. We showed that the three-body interactions encoded microscopically in nonlinear couplings give rise to added dynamic phenomena occurring beyond the pairwise interactions.[59] We also identified various types of phase transitions toward synchrony and established the universal scaling relation for each branch of multiclusters near the critical points.[60]

*c. Heterogeneous and nonlinear coupling.* Beyond the uniform coupling, the heterogeneous interactions have attracted particular attention, when the classic Kuramoto model was generalized by incorporating additional effects. Such a consideration is motivated by the fact that, in many realistic applications, there will inevitably be some variations among the oscillators. For instance, both the intrinsic nonidentical natural frequencies and the network topology represent a sort of inhomogeneity of the coupled system. The remarkable dynamic consequence of correlating these two types of heterogeneity is the emergence of explosive synchronization,[61,62] which is characterized by the discontinuous transition between the disordered and coherent states. Investigating such an abrupt dynamic transition has provided the theoretical underpinning for analyzing the dynamic structure and system function.[63–67] Almost all the works have so far focused on exploring how the collective dynamics is shaped by various heterogeneous schemes. However, further investigation of the impacts of the coupling strategies on synchronization dynamics as

well as the critical behavior for its onset or vanishing remains poorly understood.

We recently considered a generalized Kuramoto model of globally coupled phase oscillators by correlating the quenched disorder of the natural frequencies and coupling strength.[68] We reveal that coupling strategies, and the correlation exponent, as well as the form of frequency distribution can greatly alter the synchronized dynamics. We systematically clarify that both the synchronized dynamics and the backward critical points manifesting the desynchronization transition are significantly shaped by coupling strategies, the correlation exponent, and frequency distribution. Our analysis gives the hints that can actually induce the phase transition, thereby providing a strategy for better manipulating or controlling synchronization in complex networks.

*d. High-dimensional oscillator dynamics.* For a better understanding of the mechanisms of synchronization, Ritort[69] introduced a solvable model of interacting random tops incorporating the orientational degree of freedom, which, in fact, extends the Kuramoto model with noise to three dimensions.[70] Later on, the $D$-dimensional Kuramoto model has been further proposed,[71,72] where all the individual oscillators (agents) are interpreted as D-dimensional unit vectors, rotating on the surface of the D-dimensional sphere.

Quite recently, Chandra *et al.*[73] systematically examined the dynamics of the D-dimensional generalized Kuramoto model with heterogeneous natural rotations; in particular, they unveiled that the nature of phase transition for the generalized Kuramoto model with an odd number of dimensions is remarkably different from that in even dimensions. Since then, there has been a burst of appealing works devoted to the study of the D-dimensional generalized Kuramoto model and its variants.[74–77]

Zou *et al.* recently proposed a new model of globally coupled D-dimensional generalized limit-cycle oscillators,[78] which explicitly incorporates both the phase and amplitude dynamics of individual units. The model includes the $D$-dimensional Kuramoto phase model as a special case in the weak coupling limit. They showed that the model for the practically important case of $D = 3$ is solvable in the thermodynamic limit, which provides a new paradigmatic example of analytically tractable models.

Another interesting and tractable example is the effect of many-body interaction on high-dimensional phase oscillators.[79] Kovalenko *et al.* showed that a population of pure contrarian globally coupled $D$-dimensional Kuramoto oscillators reaches a collective synchronous state when the interplay between the units goes beyond the limit of pairwise interactions. They found that the presence of higher-order interactions may induce the appearance of a coherent state even when the oscillators are coupled negatively to the mean field.

*e. Second-order dynamics: Inertia effect.* The inertia effect on collective phase dynamics is an important topic and can be traced back to the work of Ermentrout by introducing inertia terms to describe synchronization among tropical Asian species of fireflies.[80] The second-order Kuramoto model has been extensively studied in recent years relating to various backgrounds such as Asian species of fireflies, Josephson-junction arrays, goods markets, and dendritic neurons.

Recent studies of second-order coupled phase oscillator dynamics are shown to find immense applications in synchronization and stability of modern distributed power grids. The decentralization of generators is the dominant property of modern power grids, which comes from large numbers of relatively small power supplies such as wind, photovoltaic, and biogas (see the review article[81]). Filatrella *et al.* first obtained the second-order Kuramoto-like dynamical equations of power grids in terms of flow and swing equations.[82] The synchronization dynamics and its stability on power grids exhibit multistable dynamics, and these issues were comprehensively investigated in terms of the basin-stability analysis.[83–85] The power-grid synchronization is closely connected to the topological properties of power grids, and the emergent failure and cascades on power networks were revealed throughout this decade.[86] The predesign of the power-grid topology has been revealed to be able to greatly optimize the synchronizability and stability of decentralized power grids.[43,87–89]

Theoretical approaches on the order-parameter dynamics in second-order Kuramoto system have long been a difficult issue. Tanaka *et al.*[90] applied the SC approach to study synchronization transitions in the second-order Kuramoto oscillators. Various properties such as hysteresis and abrupt transitions, oscillatory states, cluster explosive synchronization, and non-equilibrium steady states were revealed. A theoretical breakthrough of the second-order phase dynamics was recently made by Gao and Efstathiou.[91,92] By improving the SC methods, correct SC equations for the second-order oscillators were obtained, which not only coincide with numerical simulations and stability analysis but also converge to the zero-inertia limit. The improved SC approach was successfully applied to the analysis on abrupt synchronization transitions, hysteresis, collective oscillatory states, partial synchronization, frustration effects,[91] and general network topologies.[92]

*f. Oscillator-network-based Ising machine.* It is insightful to emphasize the phase-dynamics description in applying to various issues related to oscillatory behaviors. One of the recently inspiring developments is the application of the modified Kuramoto model to solving combinatorial optimization (CO) problems.[93,94] This idea comes from the efforts in designing electronic devices and computing architectures to sustain the performance advancement of computing and to challenge the breakdown of Moore's law. The Ising machine was proved to be a non-von-Neumann solver and has received wide attention in recent years. It is capable of solving intractable CO problems, which are difficult to be solved using conventional digital computers. In fact, many CO problems can be mapped to finding the corresponding ground states of the Ising model.

Wang *et al.* proposed a type of oscillator Ising machine (OIM) to make Ising machines by using networks of coupled self-sustaining nonlinear oscillators.[95,96] A natural realization of the spin states in OIM can be described by ground-state patterns in coupled phase oscillators. To accomplish this in terms of the Kuramoto model, the binarization of phases for oscillators is necessary. This can be

implemented by introducing a $\pi$-periodic coupling term, e.g., a term with the form $\sin(2\theta_i)$ in the phase dynamics.

Compared with other types of Ising solvers, OIM possesses its advantages in fast solving speed and low power consumption. Because there have been numerous implementations of nano-spintronic and memristive nanoscale oscillators in experiments,[97–99] theoretical and meanwhile experimental studies of this topic is a challenging and promising subject.[100] As compared with other well-developed digital systems, the oscillator-network-based Ising machines are still relatively primitive in terms of performance, hardware cost, and complexity. In the near future, OIMs should have the advantages of high integration density, low power consumption, and fast solving speed, and wide spectra of applications in mobile edge devices and data centers are expected.[94]

## IV. ORDER-PARAMETER APPROACH TO CHIMERA STATES

### A. The spatially extended frustrated Kuramoto model

As an application of order-parameter dynamics to coupled phase oscillators, let us investigate an interesting spatiotemporal behavior with coexisted coherent-incoherent patterns, called the *chimera state*. This phenomenon was first reported by Kuramoto and Battogtokh in nonlocally coupled phase oscillators.[101] The initial version of tractable models was studied in coupled phase oscillator systems. In this section, we discuss chimera dynamics of the Kuramoto model with nonlocal coupling in terms of order-parameter analysis and the theoretical frameworks of the Ott–Antonsen approach.

A spatially extended phase equation that can be reduced from the spatially one-dimensional Ginzburg–Landau equation is often adopted to investigate the collective behavior of chimera states,

$$\frac{\partial\theta(x,t)}{\partial t} = \omega - \int_0^L G(x-x')\sin[\theta(x,t) - \theta(x',t) + \alpha]dx'. \quad (58)$$

Here, $x \ni [0,1]$ denotes the spatial position, and $\theta(x,t)$ is the instantaneous phase of the oscillator at $x$. One usually adopts the periodic boundary condition, i.e., $\theta(x+L) = \theta(x,t)$. Oscillators are set to be spatially identical, i.e., $\omega(x) = \omega = 0$ without loss of generality. The frustration $\alpha$ measures the natural mismatch among the phases of oscillators located at $x$ and $x'$. The emergence of chimera states requires that $\alpha$ is chosen at the edge of asynchrony, i.e., $\alpha \lesssim \pi/2$.

The coupling function $G(X)$ defines the non-local coupling between oscillators at $x$ and $x'$, where $X = x - x'$. The function $G(X)$ is assumed to be symmetric ($G(-X) = G(X)$), positive ($G(X) \geq 0$), decreasing ($G'(|X|) \leq 0$), and normalized $\left(\int_{-\infty}^{\infty} G(X)dX = 1\right)$. Previous studies had considered several different forms of coupling functions $G$, e.g.,the exponential kernel[101] with $\kappa > 0$ considered by Kuramoto *et al.*,

$$G(X) \propto \exp(-\kappa|X|), \quad (59)$$

the cosine kernel[102,103] proposed by Strogatz *et al.*,

$$G(X) = \frac{1 + A\cos(X)}{2\pi}, \quad (60)$$

with $A < 1$ and the piecewise-constant coupling functions[104,105] with a radius $\gamma \in (0,1)$ as

$$G(X) = \begin{cases} \dfrac{1}{2\pi\gamma}, & |x| \leq \pi\gamma, \\ 0, & |x| > \pi\gamma. \end{cases} \quad (61)$$

A typical manifestation of the chimera state is shown by a snapshot of the phase profile $\theta(x,t)$ at $t$ in Fig. 1(a) for the coupling function form given by (60). It can be found that the coherent region coexists with the incoherent segment. The oscillators near $x = \pm\pi$ evolve nearly in phase, while the scattered oscillators are drifting, and their motions are strongly nonuniform, i.e., they move with the same constant frequency. By introducing the reference frame rotating at the angular frequency $\Omega$, the phase variables can be rewritten as $\theta_i - \Omega t \to \theta_i$. When the chimera state emerges, $\Omega$ can be chosen to be the average frequency of the oscillators in the coherent subset. Figure 1(b) is the snapshot of velocity $v = \partial\theta(x,t)/\partial t$ of oscillators, which indicates that the oscillators in coherent regions are rotating with the same velocity.

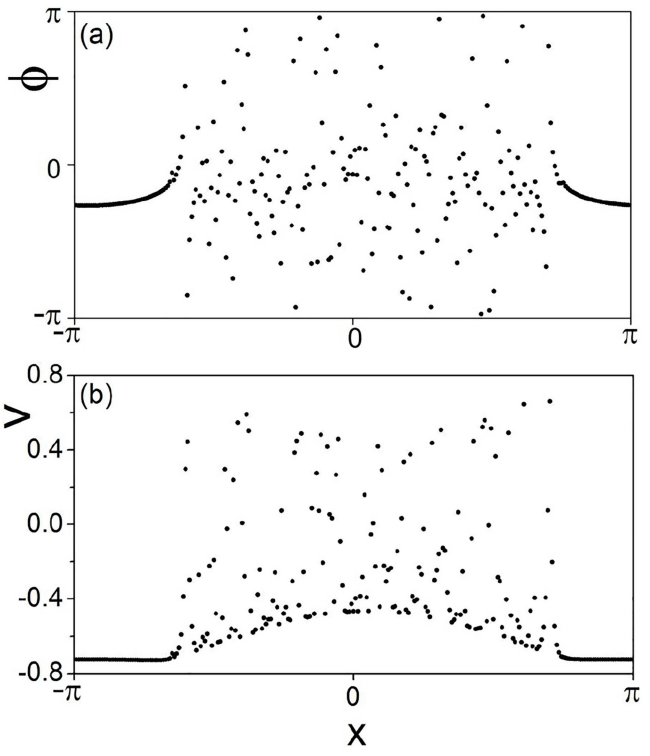


**FIG. 1.** Demonstration of the chimera state in system (58) with the kernel function $G(x-x') = (1 + A\cos(x-x'))/(2\pi)$. (a) An instantaneous snapshot of the phase profile $\theta(x)$. (b) An instantaneous snapshot of the phase velocity profile $v(x)$. Reproduced with permission from N. Yao and Z. G. Zheng, Int. J. Mod. Phys. B **30**, 1630002 (2016). Copyright 2016 World Scientific Publishing.[164]

A local complex order parameter $Z$ characterizing the collective dynamics of oscillators is defined for oscillators at position $x$,

$$Z(x,t) \equiv R(x,t)e^{i\Theta(x,t)} = \int G(x-x')e^{i\theta(x',t)}dx'. \quad (62)$$

The modulus $R$ depends not only on the phase coherence around the position $x$ but also on the distribution of coupling strengths given by the function $G$, and $\Theta$ represents the local averaged phase at $x$.

Kuramoto and Battogtokh[101] proposed the SC scheme to study the dynamics of chimera states. Abrams *et al.* adopted the Ott–Antonsen ansatz to analyze the dynamics of chimera states that emerged in the system composed of two subnetworks.[106] Laing[107] derived equations to describe the dynamics of a class of chimera states by means of the Ott–Antonsen ansatz.

### B. The Ott-Antonsen approach to chimeras

The state of the system at time $t$ is described by introducing the distribution function $\rho(x,\theta,t)$ satisfying the continuity equation

$$\frac{\partial \rho}{\partial t} + \frac{\partial}{\partial \theta}(\rho v) = 0. \quad (63)$$

Here, the velocity field

$$v(x,t) = \omega - \iint dx'd\theta' G(x-x')\sin(\theta-\theta'+\alpha)\rho(x',\theta',t), \quad (64)$$

and $\theta = \theta(x)$ and $\theta' = \theta(x')$. The complex order parameter is reformulated as

$$Z(x,t) \equiv R(x,t)e^{i\theta(x,t)} = \int dx' G(x-x')\int_{-\pi}^{\pi} d\theta' e^{i\theta'}\rho(x',\theta',t). \quad (65)$$

Equation (64) can then be expressed by using (65) as

$$v(x,t) = \omega - \frac{1}{2i}\left[\bar{Z}(x,t)e^{i(\theta+\alpha)} - Z(x,t)e^{-i(\theta+\alpha)}\right]. \quad (66)$$

Expanding $\rho(x,\theta,t)$ into Fourier series and considering the Ott–Antonsen ansatz for Fourier coefficients, one has

$$\rho(x,\theta,t) = \frac{1}{2\pi}\left\{1 + \sum_{n=1}^{\infty}\left[h_n(x,t)e^{in\theta} + \text{c.c.}\right]\right\} = \frac{1}{2\pi}\left\{1 + \sum_{n=1}^{\infty}\left[h^n(x,t)e^{in\theta} + \text{c.c.}\right]\right\}, \quad (67)$$

where the OA ansatz requires $h_n(x,t) = h^n(x,t)$. Inserting Eq. (67) into the continuity Eq. (63) and comparing the coefficient of the term $e^{in\theta}$, one obtains

$$\frac{\partial h(x,t)}{\partial t} = -i\omega h(x,t) + \frac{1}{2}\left[\bar{Z}(x,t)e^{i\alpha} - Z(x,t)e^{-i\alpha}h^2(x,t)\right]. \quad (68)$$

Substituting Eq. (67) into Eq. (65), we obtain the order parameter as

$$Z(x,t) = \int dx' G(x-x')\int_{-\pi}^{\pi} d\theta' e^{i\theta'} \times \frac{1}{2\pi}\left\{1 + \sum_{n=1}^{\infty}\left[h^n(x',t)e^{in\theta'} + \bar{h}^n(x',t)e^{-in\theta'}\right]\right\}. \quad (69)$$

Because $\int_{-\pi}^{\pi} e^{im\theta}d\theta = 0$ for $m \neq 0$, one has from (69),

$$Z(x,t) = \int dx' G(x-x')\bar{h}(x',t). \quad (70)$$

The order parameter $Z$ obtained above can characterize the spatiotemporal pattern of chimera states. Furthermore, the significance of the quantity $h$ can exhibit the coherent and incoherent regions in a chimera state.[107]

Similar to the discussions in Sec. III, the distribution defined by Eq. (67) has a clear physical interpretation with respect to the complex-valued function $h$. The probability density function $\rho(\theta)$ at position $x$ has proportionality

$$\rho(\theta) \sim \sum_{n=-\infty}^{\infty}[h(x)]^n e^{in\theta}. \quad (71)$$

By summing over the geometric progression, for any $|h(x,t)| \leq 1$, we have

$$\rho(\theta) = \frac{1-|h|^2}{2\pi[1-2|h|\cos(\theta-\arg h)+|h|^2]}, \quad (72)$$

which is a Poisson kernel. In particular, the angle $\arg h$ determines the location of the distribution center, whereas $|h|$ characterizes the degree of non-uniformity, as shown in Fig. 2.

However, if $|h| = 1$, Eq. (72) degenerates into a Dirac delta function $\rho(\theta) = \delta(\theta - \arg h)$, which corresponds to a phase-locking, thus $\theta$ gives the value of $\arg h$ at which the maximum of $\rho$ occurs, and $|h|$ is a measure of the peakedness of the distribution.

On the other hand, for any $f$ given by Eq. (67),

$$h(x,t) = \int_{-\pi}^{\pi} d\theta \rho(x,\theta,t)e^{i\theta}. \quad (73)$$

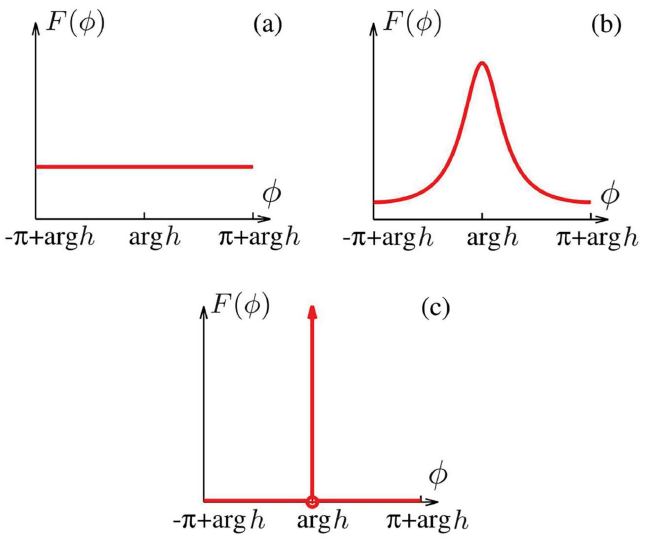


**FIG. 2.** The Poisson distributions $F(\theta)$. (a) $|h| = 0$, (b) $0 < |h| < 1$, and (c) $|h| = 1$. Reproduced with permission from O. E. Omel'chenko, Nonlinearity **26**, 2469 (2013). Copyright 2013 IOP Publishing.

The function $h(x,t)$ defined in Eq. (73) measures the synchronization degree of oscillators around point $x$; hence, it can also be considered as a *local order parameter*.

If $|h(x,t)| = 1$ at some $x$, oscillators with $x \approx x \pm \epsilon$ ($\epsilon \to 0$) are phase-locked. If $|h(x,t)| < 1$ at some $x$, oscillators at $x \approx x \pm \epsilon$ are phase incoherent. Moreover, there exist continuous symmetries in Eq. (68) under the spatial translation transformation $h(x,t) \mapsto h(x+s,t)$, $s \in \mathbb{R}$, and phase rotation $h(x,t) \mapsto h(x,t)e^{i\vartheta}$. Therefore, $h(x,t)$ can be considered as a rotating wave solution[108] with the form

$$h(x,t) = a(x)e^{-i\Omega t}, \tag{74}$$

with $\Omega$ being the collective frequency and $a(x)$ being the spatial profile. The probabilistic interpretation of the local order parameter $h$ requires $|a(x)| \leq 1$ for all $x$, and the regions with $|a(x)| = 1$ and $|a(x)| < 1$ as to be coherent and incoherent, respectively.

Substituting (74) into (68), one obtains

$$-i(\omega - \Omega) + \frac{1}{2}[\bar{\Xi}(x)e^{i\alpha} - \Xi(x)e^{-i\alpha}a(x)^2] = 0, \tag{75}$$

where

$$\Xi(x) = \int dx' G(x-x')\bar{a}(x'). \tag{76}$$

$a(x)$ can be obtained from (75) as

$$a(x) = \begin{cases} \dfrac{-i(\omega-\Omega) + \sqrt{-(\omega-\Omega)^2 + |\Xi(x)|^2}}{\Xi(x)e^{-i\alpha}} & for\ |\Xi(x)| \geq |\omega - \Omega|, \\ \dfrac{-i(\omega-\Omega) + i\sqrt{(\omega-\Omega)^2 - |\Xi(x)|^2}}{\Xi(x)e^{-i\alpha}} & for\ |\Xi(x)| < |\omega - \Omega|. \end{cases}$$

Inserting $a(x)$ into (76) and writing the complex parameter as $\Xi(x) \equiv \tilde{R}(x)e^{i\tilde{\Theta}(x)}$, one has

$$\tilde{R}(x)e^{i\tilde{\Theta}(x)} = e^{-i\alpha}\int dx' G(x-x')e^{i\tilde{\Theta}(x)} \times \frac{i(\omega-\Omega) + \sqrt{\tilde{R}^2(x') - (\omega-\Omega)^2}}{\tilde{R}(x')} \tag{77}$$

for $\tilde{R}(x) \geq |\omega - \Omega|$, and

$$\tilde{R}(x)e^{i\tilde{\Theta}(x)} = ie^{-i\alpha}\int dx' G(x-x')e^{i\tilde{\Theta}(x)} \times \frac{(\omega-\Omega) - \sqrt{(\omega-\Omega)^2 - \tilde{R}^2(x')}}{\tilde{R}(x')} \tag{78}$$

for $\tilde{R}(x) < |\omega - \Omega|$. Introducing parameters $\beta = \frac{\pi}{2} - \alpha$ and $\Delta = \omega - \Omega$, the above expressions can be unified as

$$\tilde{R}(x)e^{i\tilde{\Theta}(x)} = e^{i\beta}\int G(x-x')e^{i\tilde{\Theta}(x')}H(x')dx', \tag{79}$$

with $H(x) = \left[\Delta - \sqrt{\Delta^2 - \tilde{R}(x)^2}\right] \Big/ \left[\tilde{R}(x)\right]$. Equation (79) is the stationary solution and can also be derived from the traditional SC approach.

The SC equation (79) can be used to solve three quantities $R(x)$, $\Theta(x)$, and the real number $\Delta$ interms of an iterative scheme in the functional space.

Figure 3 gives the order parameter $R(x)$, $\Theta(x)$, and the real number $\Delta$ obtained from [Eq. (79)]. It can be found that the part satisfying $R(x) \geq |\Delta|$ corresponds to the phase-lock domain in Fig. 1.

Over the past decades, there have been extensive progresses in studies of chimeras. It has been revealed that chimera states can

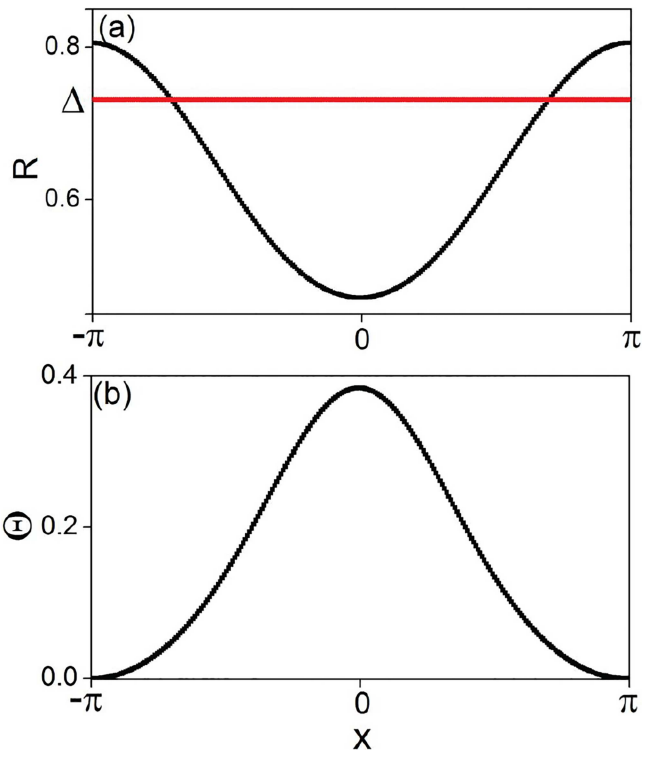


**FIG. 3.** (a) Modulus $R(x)$ of complex order parameter and real number $\Delta$ obtained from Eq. (79), where $R(x) \geq |\Delta|$ corresponds to the coherent domain. (b) Argument $\Theta(x)$ of the oscillators obtained from Eq. (79). Reproduced with permission from N. Yao and Z. G. Zheng, Int. J. Mod. Phys. B **30**, 1630002 (2016). Copyright 2016 World Scientific Publishing.[164]

be observed not only in coupled phase oscillators but also in other systems with distinct local dynamics, such as discrete maps,[109] continuous chaotic systems,[110] bursting neurons,[111] and even bistable models.[112] New types of chimera modes, such as breathing,[106] spiral-wave,[113] multiple,[114] death chimeras,[115] as well as amplitude and amplitude-mediated chimeras,[116] have been revealed. These explorations greatly extended the conceptual scope of the chimera state.

Furthermore, the potential applications of chimera states in nature are related to many vital physiological processes, such as the unihemispheric sleep of some marine mammals,[117] the first-night effect in human sleep,[118] and epileptic seizures.[119] Studies of chimera dynamics and its functioning have now become a central topic in the interdisciplinary field of neuroscience and life science.[8]

## V. ORDER-PARAMETER THEORY OF NEURON NETWORK DYNAMICS

The understanding of the emergence of brain function from the collective dynamics of networks of spiking neurons is a major goal of the applications of statistical physics and nonlinear dynamics to neuroscience.[12,120,121] Extensive explorations have been addressed in the past decades through exploring large-scale experimental data and performing numerical simulations.[122–124]

Mean-field theories have been phenomenologically proposed to gain insights into macroscopic states of large neuronal networks in terms of the collective firing activity of the neurons, or the firing rate,[125,126] which were considered as macroscopic order parameters. However, establishing an exact theoretical correspondence between the firing rate of neural networks and the underlying microscopic state of the spiking neurons was not realized until the recent work by Montbrió *et al.*[9] The central idea of the Montbrio–Pazo–Roxin (MPR) approach is to apply the Lorentz ansatz and derive exact macroscopic equations for networks of spiking neurons. It was revealed that the spike generation mechanism of individual neurons introduces an effective coupling between the firing rate and the mean membrane potential governing the evolution of the neuronal network. The MPR approach can exactly describe all possible macroscopic dynamical states of the network, including states of synchronous spiking activity. Moreover, the firing-rate description is closely related to the Ott–Antonsen theory[6,7] in describing synchrony dynamics of coupled phase oscillators.

### A. The quadratic integrate-and-fire neuron population model

One adopts the quadratic integrate-and-fire (QIF) neuron model to study the collective firing patterns on neural networks, which makes an analytical argument attainable. A QIF neuron is a canonical model for class I neurons in describing the dynamics near the spiking threshold. The microscopic dynamics of the population of QIF neurons is given by the evolution of the membrane potentials $V_j, j = 1, 2, \ldots, N$ as

$$\dot{V}_j = V_j^2 + I_j, \tag{80}$$

where $V_j$ and $I_j$ represent the membrane potential of the $j$th neuron and the input current, respectively. The membrane potential is reset to the rest potential $V_j \leftarrow V_r$ as long as the potential $V_j$ exceeds a peak value $V_p$. When the membrane potential of the $j$th neuron $V_j$ reaches the peak value $V_p$, the neuron experiences a spiking, and its voltage is then reset to $V_r$. For convenience here the limit $V_p = -V_r \to \infty$ is adopted. The input currents in (80) includes the following different inputs:

$$I_j = \eta_j + Js(t) + I(t), \tag{81}$$

where $\eta_j$ is the external heterogeneous, quenched input, and $I(t)$ is the common time-varying current, and the mean-field input $Js(t)$ comes from the synaptic input from other connected neurons, where $J$ is the synaptic weight, and $s(t)$ represents the mean synaptic activation and is written as

$$s(t) = \frac{1}{N}\sum_{j=1}^{N}\sum_{k}^{t_j^k<t}\int_{-\infty}^{t} a_\tau(t-t')\delta\left(t'-t_j^k\right). \tag{82}$$

Here, a non-zero contribution from the $j$th neuron is adopted if a spike with the Dirac delta function $\delta(t)$ occurs at $t_j^k$, and $a_\tau(t)$ is the normalized synaptic activation caused by a single presynaptic spike with time scale $\tau$, e.g.,

$$a_{\tau(t)} = \frac{1}{\tau}e^{-t/\tau}. \tag{83}$$

### B. The Lorentz ansatz

Consider a very large population of $N$ QIF neurons. In thermodynamic limit $N \to \infty$, one may replace the above microscopic description by introducing the conditional distribution function $\rho(V, t; \eta)$ as the fraction of neurons with membrane potentials between $V$ and $V + dV$ for a given $\eta$ at time $t$. Parameter $\eta$ is usually assumed to be random and obeys the probability distribution function $g(\eta)$. The total voltage density at time $t$ is then given by

$$\rho(V, t) = \int_{-\infty}^{\infty} \rho(V, t; \eta)g(\eta)d\eta. \tag{84}$$

The evolution of the distribution function $\rho(V, t; \eta)$ obeys the following continuity equation:

$$\frac{\partial\rho(V,t;\eta)}{\partial t} + \frac{\partial}{\partial V}\left[\left(V^2 + \eta + Js + I\right)\rho(V, t; \eta)\right] = 0. \tag{85}$$

For the case of $I(t) = 0$, the trivial stationary solution of the continuity equation for each given value of $\eta$ has the following Lorentzian-function form:

$$\rho_0(V; \eta) \propto \frac{1}{V^2 + \eta + Js}. \tag{86}$$

This Lorentzian density physically implies that the membrane voltages of firing neurons with the same $\eta$ value are distributed with a density inversely proportional to $\dot{V}$ [see Eq. (80)]. For those $\eta$ values corresponding to quiescent neurons, the density $\rho_0(V; \eta)$ collapses at the rest state in the form of a Dirac delta function.

The MPR approach introduces the Lorentz ansatz to further deal with general cases. It is assumed that, independent of initial conditions, solutions of Eq. (85) generically converge to a

Lorentzian-shaped function as

$$\rho(V,t;\eta)=\frac{1}{\pi}\frac{x(\eta,t)}{[V-y(\eta,t)]^2+x(\eta,t)^2}, \tag{87}$$

where the Lorentzian function possesses the time-dependent half-width $x(\eta,t)$ and center at $y(\eta,t)$.

### C. Macroscopic dynamics: Firing-rate equations

The distribution in (87) indicates that the Lorenz ansatz Eq. (87) can completely describe the macroscopic dynamics of the network of QIF neurons. It is important to understand the evolutionary dynamics of the factors $x(\eta,t)$ and $y(\eta,t)$.

In fact, the half-width $x(\eta,t)$ of the Lorenz distribution (87) has a simple relation with the firing rate of the populations of neurons. The firing rate $r(\eta,t)$ denotes the number of spikes per unit time and can be computed by noting that neurons fire at a rate given by the probability flux at infinity,

$$r(\eta,t)=\rho(V\to\infty,t;\eta), \tag{88}$$

where the limit $V\to\infty$ can be evaluated within the Lorenz ansatz and gives the following identity:

$$x(\eta,t)=\pi r(\eta,t). \tag{89}$$

Then, the total firing rate $r(t)$ can be worked out from $x(\eta,t)$ that

$$r(t)=\frac{1}{\pi}\int_{-\infty}^{\infty}x(\eta,t)g(\eta)d\eta. \tag{90}$$

The center of the Lorentzian distribution $y(\eta,t)$ can be computed by the mean of the membrane potential of all neurons as

$$y(\eta,t)=\int_{-\infty}^{\infty}\rho(V,t;\eta)VdV. \tag{91}$$

The integral can be performed by taking the Cauchy principal value defined as

$$y(\eta,t)=\mathbf{P}\int_{-\infty}^{\infty}V\rho(V,t;\eta)dV=\lim_{R\to\infty}\int_{-R}^{R}V\rho(V,t;\eta)dV. \tag{92}$$

The mean membrane potential is then given by summing over all possible $\eta$ by

$$v(t)=\int_{-\infty}^{\infty}y(\eta,t)g(\eta)d\eta. \tag{93}$$

Substituting the Lorentz ansatz equation (87) into the continuity equation (85) and introducing

$$w(\eta,t)\equiv x(\eta,t)+iy(\eta,t), \tag{94}$$

one obtains the following complex equation:

$$\frac{\partial w(\eta,t)}{\partial t}=i\left[\eta+Js(t)-w(\eta,t)^2+I(t)\right]. \tag{95}$$

The closeness of Eq. (95) demands that the mean synaptic activation $s(t)$ can be expressed as a function of $w(\eta,t)$. By considering the simplest case of an infinitely fast synapses, $\tau\to 0$ in Eq. (83), one gets the firing rate $s(t)=r(t)$. Therefore, the dynamics of coupled QIF neurons can be reduced to Eq. (95) with a low-dimensional description.

By considering the Lorentzian distribution of $g(\eta)$ with half-width $\Delta$ centered at $\bar{\eta}$,

$$g(\eta)=\frac{1}{\pi}\frac{\Delta}{(\eta-\bar{\eta})^2+\Delta^2}, \tag{96}$$

the integrals in Eqs. (90) and (93) can be worked out in the complex $\eta$ plane using the residue theorem. The firing rate and the mean membrane potential depend on the value of $w$ at the pole of $g(\eta)$ in the negative half $\eta$ plane as

$$\pi r(t)+iv(t)=w(\bar{\eta}-i\Delta,t). \tag{97}$$

By setting $\eta=\bar{\eta}-i\Delta$ in Eq. (95), one eventually obtains the firing-rate equations (FREs) as the following two ordinary differential equations:

$$\dot{r}=\Delta/\pi+2rv, \tag{98a}$$

$$\dot{v}=v^2+\bar{\eta}+Jr+I(t)-\pi^2r^2. \tag{98b}$$

This nonlinear system describes the macroscopic dynamics of the population of QIF neurons in terms of the population firing rate $r$ and mean membrane potential $v$. Therefore, Eq. (98) is the order-parameter equation and describes the effect of the single-cell spike generation and reset mechanism at the network level. As shown in Figs. 4(a)–4(d), numerical simulations well support this order-parameter description.[9] Moreover, rich collective dynamics are demonstrated in Fig. 4(e) at the macroscopic level.

The Lorentz ansatz is closely related to the Ott–Antonsen ansatz and the Watanabe–Strogatz transformation. By introducing the phase variable related to the voltage of the QIF neuron as

$$V_j=\tan(\theta_j/2), \tag{99}$$

one obtains an ensemble of Theta neurons with the phase oscillator description from the QIF neurons (80) as

$$\dot{\theta}_j=(1-\cos\theta_j)+(1+\cos\theta_j)\left[\eta_j+Js(t)+I(t)\right]. \tag{100}$$

In the new phase variable $\theta\in[0,2\pi)$, the Lorentz ansatz given by Eq. (87) becomes

$$\rho(\theta;\eta,t)=\frac{1}{2\pi}\mathrm{Re}\left[\frac{1+\alpha(\eta,t)e^{i\theta}}{1-\alpha(\eta,t)e^{i\theta}}\right]. \tag{101}$$

Here, $\alpha(\eta,t)$ is related to $w(\eta,t)$ as

$$\alpha(\eta,t)=\frac{1-w(\eta,t)}{1+w(\eta,t)}. \tag{102}$$

Parameter $\alpha$, in fact, measures the uniformity of the phase density. Obviously, $\alpha=0$ in Eq. (101) yields a perfectly uniform density $\rho(\theta;\eta,t)=\frac{1}{2\pi}$. A larger value of $\alpha$ reflects a larger interference of the phase variable $\theta$ in the distribution, i.e., the non-uniformity of the phase density.

Therefore, the description of dynamics in the $\{\theta_i\}$ state space and the $\{\theta_i\}$ state space is equivalent. They represent the dynamics of the same system in $V$-representation and $\theta$-representation of the so-called Poisson kernel, with the voltage variables on the half-plane and the phase variables on the unit disk, respectively. These two representations are related through the transformation Eq. (102), which is a conformal mapping from the half-plane $\mathrm{Re}(w)\geq 0$ onto the unit disk $|\alpha|\leq 1$.

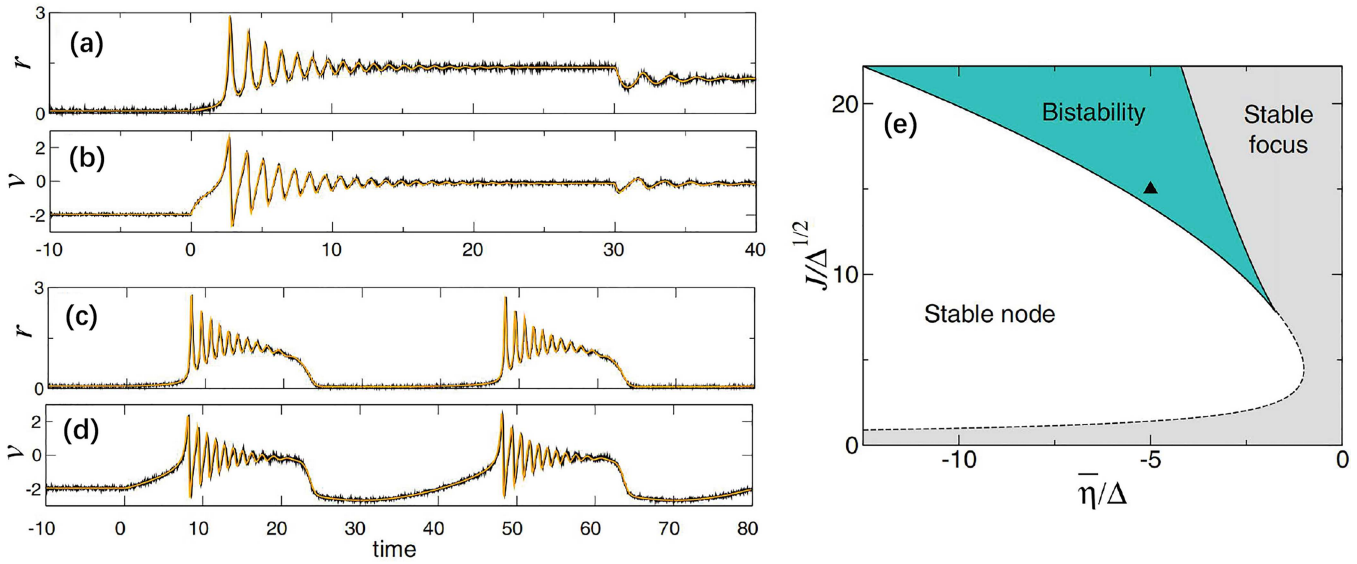


**FIG. 4.** (a)–(d) The transient dynamics of an ensemble of QIF model neurons. (e) Phase diagram of the FRE. $r(t)$ is instantaneous firing rate, $v(t)$ is the mean membrane potential. Black lines are the simulation of networks of $N = 10^4$ QIF neurons, and orange lines are simulations of the FRE. (a)–(b) Dynamics driven by $I = 3$; (c)–(d) dynamics driven by $I(t) = I_0 \sin(\omega t)$, where $I_0 = 3.0$ and $\omega = \pi/20$. Parameters: $J = 5$, $\bar{\eta} = -5$, and $\Delta = 1$. Reproduced with permission from Montbrió *et al.*, Phys. Rev. X **5**, 021028 (2015). Copyright 2015 American Physical Society.

Moreover, the Lorentz ansatz in Eq. (87) is just the ansatz discovered in 2008 by Ott and Antonsen.[6] According to the OA theory, in the thermodynamic limit, the dynamics of the system is

$$\frac{\partial \theta(\eta,t)}{\partial t} = \omega(\eta,t) + \mathrm{Im}\left[h(\eta,t)e^{-i\theta}\right], \tag{103}$$

which generally converges to the OA manifold. For the case of Eq. (100), one has

$$\omega(\eta,t) = 1 + \eta + Js + I$$

and

$$h(\eta,t) = i(-1 + \eta + Js + I).$$

Let us discuss the relation between the firing rate and Kuramoto order parameter. In fact, one can build a mapping between the collective variables describing neuronal dynamics $(r, v)$ and the Kuramoto order parameter $Z$ describing collective phase coherence of coupled oscillators. For each given parameter $\eta$, Eq. (102) relates the firing rate and the mean membrane potential that are expressed in $w = \pi r + iv$ to $\alpha$ signifying the phase-distribution uniformity. The Kuramoto order parameter is then obtained by integrating $\alpha$ over the whole population as

$$Z(t) = \int_{-\infty}^{\infty} g(\eta) \int_0^{2\pi} \rho(\theta;\eta,t)e^{i\theta}\, d\theta\, d\eta = \int_{-\infty}^{\infty} g(\eta)\alpha^*(\eta,t)\, d\eta. \tag{104}$$

Here, the density $\rho(\theta;\eta,t)$ is assumed to be the OA ansatz equation (101). For a Lorentzian distribution of currents $g(\eta,t)$, an exact formula of Eq. (104) can be obtained as

$$Z = \frac{1 - W^*}{1 + W^*}. \tag{105}$$

This formula relates the Kuramoto order parameter $Z$ with the firing-rate quantity $W = \pi r + iv$.

The MPR approach has been extensively adopted and applied to studies of collective oscillations and synchronization dynamics of coupled neuronal systems. Ratas and Pyragas studied the macroscopic self-oscillations and aging transition in a network of synaptically coupled quadratic integrate-and-fire neurons.[127,128] They also analyzed the dynamics of two coupled identical populations of quadratic integrate-and-fire neurons and revealed rich varieties of dynamics, such as splay state, antiphase periodic oscillations, chimera-like states, and chaotic oscillations as well as bistability between various states. Dynamics such as the quasiperiodic synchronization and collective chaos in coupled synaptically delayed inhibitory neurons were extensively studied in terms of the MPR approach.[129,130]

It has been well known that excessive synchronization can cause abnormal brain rhythms associated with neurological diseases such as Parkinson's disease, epilepsy, and tinnitus. A balanced synchrony can be realized by the coexistence of excitatory and inhibitory neurons in neural networks. Pyragas *et al.* recently investigated the collective oscillations and their suppression by external stimulation in a large-scale neural network consisting of interacting populations of excitatory and inhibitory QIF neurons.[131] They showed that high-frequency stimulation of an inhibitory population can stabilize an unstable resting state and effectively suppress collective oscillations. Similar asynchronous and coherent dynamics in

balanced excitatory-inhibitory spiking networks were also explored by Bi *et al.*[132]

The MPR reduction methodology was further extended by considering different improvements. The MPR scheme assumes that the neurons produce symmetric spikes by ignoring spike shapes. Montbrio and Pazo[133] gave an improved approach by relaxing the symmetric-spike assumption and reveal a dual role of electrical synapses as equalizing membrane potentials favoring the emergence of synchrony and as virtual chemical synapses. Goldobin *et al.* developed the MPR theory by considering non-Lorentzian deviations and introducing the pseudo-cumulants expansion, which can analytically treat dynamics of heterogeneous spiking neural networks subject to extrinsic and endogenous fluctuations.[134]

## VI. ORDER-PARAMETER DYNAMICS FROM DATA: EIGEN-MICROSTATE APPROACH

We are undergoing the era of big data. Data collected from different backgrounds are closely connected with the intrinsic and evolutionary properties of complex systems. In this section, our focus is on the studies of intrinsic macroscopic properties of complex systems when neither the microscopic modeling nor macroscopic equations are available. The information that we can obtain about the behavior of the system is the spatiotemporal data either from experiments or simulations, which vary in depth and detail. These data are complicated because they are highly entangled and non-stationary. An important question is whether there exist any approaches to extract the information of order-parameter dynamics of the system. Recent explorations indicate that statistical approaches may be crucial in revealing the order inherent in such complexity.

Recently, we proposed the so-called *eigen-microstate approach* (EMA)[21,135] in dealing with dynamics and phase transitions in complex systems across various physical backgrounds. The basic idea of the EMA approach is based on the ensemble theory of statistical physics. In this approach, the statistical ensemble composed of the microstates during an observation time interval is described by a normalized matrix. From this matrix, we can derive the eigen-microstates. A general microstate is the linear superposition of eigen-microstates with probability amplitudes equal to the corresponding eigenvalues. A finite eigenvalue in thermodynamic limits indicates the condensation of eigen-microstate and the emergence of a phase described by the eigen-microstate. This approach is a generalization of the Bose–Einstein condensation of Bose gas and can be used to study phase transitions of broad interests. The order parameter of phase transition is identified as the eigenvalue that follows a finite-size scaling form in the critical region. Accordingly, we can further calculate critical exponents of the phase transition.

From the viewpoint of self-organization theory, the EMA scheme is a practical realization of synergetics, where the destined mission is to look for the dominant eigenstates with the largest probability. In the following, we first sketch the mathematical basis of the EMA approach and then discuss some successful applications in different physical backgrounds. These seemingly different problems, essentially, are the natural consequences of the competition and self-organization of the intrinsic degrees in complex systems. The transitions among different macroscopic modes are the manifestations of the emergence.

### A. Eigen-microstate decomposition (EMD)

#### 1. Microstates and statistical ensemble

For a complex system composed of $N$ agents, we can obtain the states of the agents from experimental measurements or computer simulations. Using the states at discrete times $t = 1, 2, \ldots, M$ in sequence, we can get the state series $S_i(t)$ of agents $i = 1, 2, \ldots N$. The average state of an agent $i$ is

$$\langle S_i \rangle = \frac{1}{N} \sum_{t=1}^{M} S_i(t). \tag{106}$$

By introducing the temporal fluctuation of agents $\delta S_i(t) = S_i(t) - \langle S \rangle$, the microstate can be defined as the fluctuations of all agents, which is represented by the following $N$-dimensional vector:

$$\delta \boldsymbol{S}(t) = \begin{bmatrix} \delta S_1(t) \\ \delta S_2(t) \\ \vdots \\ \delta S_N(t) \end{bmatrix}. \tag{107}$$

A statistical ensemble of the complex system can be constructed with the $M$ microstates, which is described by an $N \times M$ matrix $\mathbf{A}$ with elements

$$A_{it} = \delta S_i(t)/\sqrt{C_0}, \tag{108}$$

where $C_0 = \sum_{t=1}^{M} \sum_{i=1}^{N} \delta S_i^2(t)$, and the column order of $\mathbf{A}$ complies with the evolution of the microstate.

#### 2. Spatial and temporal correlations

The temporal correlation between microstates at times $t$ and $t'$ can be defined as the vector product,

$$C_{tt'} = \delta \boldsymbol{S}(t)^T \cdot \delta \boldsymbol{S}\left(t'\right). \tag{109}$$

An $M \times M$ correlation matrix $\mathbf{C} = \{C_{tt'}\}$ can be written as

$$\mathbf{C} = C_0 \mathbf{A}^T \cdot \mathbf{A}, \tag{110}$$

where the trace $\mathrm{Tr}(\mathbf{C}) = \sum_{t=1}^{M} C_{tt} = C_0$.

The statistical ensemble can also be considered as an ensemble of dynamical microstates of agents, which are described by $N$ $M$-dimensional vectors

$$\delta \boldsymbol{S}_i = [\delta S_i(1), \delta S_i(2), \ldots, \delta S_i(M)], \tag{111}$$

where $i = 1, 2, \ldots, N$.

We can further introduce the spatial correlation between dynamical microstates $\delta S_i$ and $\delta S_j$ as

$$K_{ij} = \delta S_i \cdot \delta S_j^T = \sum_{t=1}^{M} \delta S_i(t) \delta S_j(t). \tag{112}$$

Then, an $N \times N$ correlation matrix $\mathbf{K} = \left\{K_{ij}\right\}$ can be written as

$$\mathbf{K} = C_0 \mathbf{A} \cdot \mathbf{A}^T, \tag{113}$$

where the trace $\mathrm{Tr}(\mathbf{K}) = \sum_{i=1}^{N} K_{ii} = C_0$.

The correlation matrix $\mathbf{C}$ has $M$ eigenvectors $\boldsymbol{V}_J$ of $J = 1, 2, \ldots, M$. With them, we can compose an $M \times M$ unitary matrix

$$\mathbf{V} = [\boldsymbol{V}_1, \boldsymbol{V}_2, \ldots, \boldsymbol{V}_M]. \tag{114}$$

### 3. Singular-value decomposition and order parameters

The correlation matrix $\mathbf{K}$ has $N$ eigenvectors $\boldsymbol{U}_I$ of $I = 1, 2, \ldots, N$. From these eigenvectors, we can obtain an $N \times N$ unitary matrix

$$\mathbf{U} = [\boldsymbol{U}_1, \boldsymbol{U}_2, \ldots, \boldsymbol{U}_N]. \tag{115}$$

According to the singular-value decomposition (SVD), the ensemble matrix $\mathbf{A}$ can be factorized as

$$\mathbf{A} = \mathbf{U} \cdot \Sigma \boldsymbol{V}^T, \tag{116}$$

where $\Sigma$ is an $N \times M$ diagonal matrix with elements

$$\Sigma_{IJ} = [V_1, V_2, \ldots, V_M], \tag{117}$$

where $r = \min(N, M)$.

Furthermore, we can rewrite the ensemble matrix $\mathbf{A}$ as

$$\mathbf{A} = \sum_{I=1}^{r} \sigma_I \mathbf{A}_I^e, \tag{118}$$

where $\mathbf{A}_I^e = \boldsymbol{U}_I \otimes \boldsymbol{V}_I$ is an $N \times M$ matrix with elements $(\mathbf{A}_I^e)_{it} = U_{iI} V_{tI}$. We call the ensemble defined by $\mathbf{A}_I^e$ an eigen-ensemble of the system. From the statistical ensemble, we can obtain not only eigen-microstate $\boldsymbol{U}_I$ but also their evolution with time $\boldsymbol{V}_I$.

From $\mathrm{Tr}(\mathbf{C}) = C_0$ or $\mathrm{Tr}(\mathbf{K}) = C_0$, we have the relation

$$\sum_{I=1}^{r} \sigma_I^2 = 1. \tag{119}$$

Therefore, we consider $\sigma_I$ as the probability amplitude and $w_I = \sigma_I^2$ as the probability of the eigen-ensemble $\mathbf{A}_I^e$ in the statistical ensemble $\mathbf{A}$. This is analogous to quantum mechanics, where a wave function can be written in terms of eigenfunctions. The square of the absolute value of expansion coefficient is the probability of the corresponding eigen-microstate.

By using $M$ eigenvectors of $\mathbf{C}$, we can obtain eigen-microstates as

$$\delta S^e(I) = \sum_{t=1}^{M} \delta S(t) V_{tI}, \tag{120}$$

where the components are expressed as

$$\delta S_I^e = \sum_{t=1}^{M} A_{it} V_{tI} = (A.V)_{iI} = (U.\Sigma)_{iI}. \tag{121}$$

Therefore, we have

$$\delta S^e(I) = \begin{cases} \sigma_I U_I & \text{for} \quad I \le r, \\ 0 & \text{otherwise.} \end{cases} \tag{122}$$

$U_I$ is the normalized eigen-microstate. These microstates are orthogonal to each other and independent.

We can further express the original microstates by eigen-microstates as

$$\delta \boldsymbol{S}(t) = \sum_{I=1}^{N} V_{tI} \delta \boldsymbol{S}^e(I) = \sum_{I=1}^{r} V_{tI} \boldsymbol{U}_I. \tag{123}$$

Using $N$ eigenvectors of $\boldsymbol{K}$, we can get the eigen-dynamical microstates[8]

$$\delta \mathbf{S}_I^e = \sum_{j=1}^{N} \delta \boldsymbol{S}_j \boldsymbol{U}_{jI}, \tag{124}$$

where the components are expressed as

$$\delta S_I^e(t) = \sum_{j=1}^{N} A_{jt} U_{jI} = \left(U^T \ldots A\right)_{It} = \left(\Sigma \ldots V^T\right)_{It}. \tag{125}$$

Further, we get

$$\delta S_I^e(t) = \begin{cases} \sigma_I V_I^T & \text{for} \quad I \le r, \\ 0 & \text{otherwise,} \end{cases} \tag{126}$$

where $V_I^T$ is the normalized eigen-dynamical microstate. Different eigen-dynamical microstates have no correlation to each other and are independent.

## B. Emergence, condensation of eigen-microstate, and phase transitions

The above framework on the eigen-microstate approach indicates that any microstate in a complex system can be expressed as a linear composition of eigen-microstates, where each coefficient denotes the occupation ratio the corresponding eigenstate. Therefore, $\sigma_I$ or $w = \sigma_I^2$ can be candidates of proper order parameters. This can be understood as follows. In a statistical ensemble without localization of microstate, the weights of all eigen-microstates are of the same order. In the limits $M \to \infty$ and $N \to \infty$, all probability amplitudes $\sigma_I \to 0$. In this case, the system is in a random and disorder state.

If a probability amplitude $\lim_{\{M,N\}\to\infty} \sigma_I \neq 0$, there exists a condensation of eigen-microstate $A_I^e$ in the statistical ensemble. This is similar to the Bose–Einstein condensation of Boson gases, where a finite proportion of infinite bosons share the lowest quantum state. This condensation indicates the appearance of a new phase in the Bose gas and there is a phase transition. The condensation of an eigen-microstate manifests that a finite proportion of infinite eigen-microstates share this eigen-microstate. A new phase appears in the system. The new phase is characterized by the eigen-microstate $U_I$. The evolution of new phase is described by $V_I$.

If $\sigma_I$ increases to finite continuously, the complex system experiences a continuous phase transition. With a jump of $\sigma_I$ at the transition point, there is a discontinuous phase transition. For a system with finite $N$, the limit of $\sigma_I$ for $M \to \infty$ can be obtained with large enough $M$. For a continuous phase transition, the distance from critical point $T_c$ is defined as $t = (T - T_c)/T_c$. In the asymptotic region with $|t| \ll 1$, we propose the finite-size form of

$\sigma_I$ as

$$\sigma_I(T,N) = N^{-\beta/d\nu} f_I\left(tN^{1/d\nu}\right), \tag{127}$$

where $\beta$ is the critical exponent of the order parameter and $\nu$ is the critical exponent of the correlation length. Correspondingly, the ratio $\sigma_2/\sigma_1$ follows the finite-size scaling form[9]

$$\sigma_2/\sigma_1 = R\left(tN^{1/d\nu}\right), \tag{128}$$

which has a fixed point at critical point $t = 0$.

In the bulk limit $N \to \infty$, we obtain the bulk order parameter,

$$\sigma_1(T,\infty) = \begin{cases} a_1(-t)^\beta & \text{for } t \le 0, \\ 0 & \text{for } t > 0. \end{cases} \tag{129}$$

## C. Applications of EMA to different systems

In the following discussions, we report some recent advances of the EMA with applications to different complex systems, which possess different backgrounds. We can find the validity and genericity of the EMA in revealing the order-parameter dynamics embedded in complexity.

### 1. Example 1: Phase transition in the Ising model

The EMA was first successfully applied to the study of equilibrium phase transitions.[135] Take the three-dimensional Ising model on a square lattice with spatial size $L \times L \times L$ as an example. The Hamiltonian is exactly written as

$$H = -J\sum_{\langle ij\rangle}^{N} S_i S_j, \tag{130}$$

where the spins $S_i = \pm 1$, and $\langle i,j\rangle$ represents the summation over all nearest-neighbor spins $j$ of the site $i$. The reduced temperature $T_c^* = k_B T_c/J$.

As the data for constructing microstates in EMA analysis, the flipping process of spins $\{\delta S_i(t) = S_i(t)\}$ can be obtained from simulating the system (130) in terms of the Wolf Algorithm. By using the above standard EMA procedure, the eigen-microstates $\boldsymbol{U}_I$ and their probabilities $w_I = \sigma_I^2$ can be worked out.

In Fig. 5, the first two probabilities $w_{1,2}$ of the two first eigenstates $\boldsymbol{U}_{1,2}$ are shown with respect to the reduced temperature $T^*$. It can be found that at higher temperatures, the probability $w_1$ of $\boldsymbol{U}_1$ is very small and comparable to other probabilities. Moreover, $w_1$ decreases to 0 as the size $L \to \infty$. With the decrease of temperature $T^*$, $w_1$ increases rapidly and becomes non-zero and size-independent as $T^*$ decreases below the critical temperature $T_c^* \approx 4.5114$, as shown in Fig. 5(a). This indicates the emergence of a new phase and the phase transition. As a comparison, the probability $w_2$ keeps much smaller than $w_1$ and decreases to 0 with increasing the system size $L$, which is clearly shown in Fig. 5(b). The ratio $w_2/w_1$ presented in Fig. 5(c) clearly shows the transition from a comparable ratio to a zero ratio as $T^*$ decreases below the critical $T_c^*$.

### 2. Example 2: Temperature fluctuations in earth systems

Due to the ubiquitous existence of nonlinear interactions and feedback loops between and within the geosphere, atmosphere, hydrosphere, cryosphere, and biosphere, the Earth operates is a typical complex system. Many climate phenomena on Earth, such as the El Ninõ and Southern Oscillation (ENSO), are closely related to the temperature fluctuations on Earth's surface and the spatial distribution of ozone at different geopotential heights.[136]

By regarding the Earth as a non-equilibrium complex system composed of many latitude-longitude grids, we studied the global temperature fluctuations of the Earth.[137] In practice, one adopts $N = 94 \times 192 = 18\,048$ grids with $1.9^\circ \times 1.875^\circ$ latitude-longitude. The microstates of the Earth as a whole are studied based on daily surface air temperature (SAT) data.[138] At a certain time $t$, the SAT at a grid $i$ is $T_i(t)$. The average SAT at the grid $i$ during a time period $M$ can be calculated as $\langle T_i\rangle = \frac{1}{M}\sum_{t=1}^{M} T_i(t)$. The fluctuation $\delta T_i = T_i(t) - \langle T\rangle$, and the standard deviation is $\Delta_i = \sqrt{\frac{1}{M}\sum_{t=1}^{M}\delta T_i(t)^2}$. Then, one can conveniently introduce the following standardized

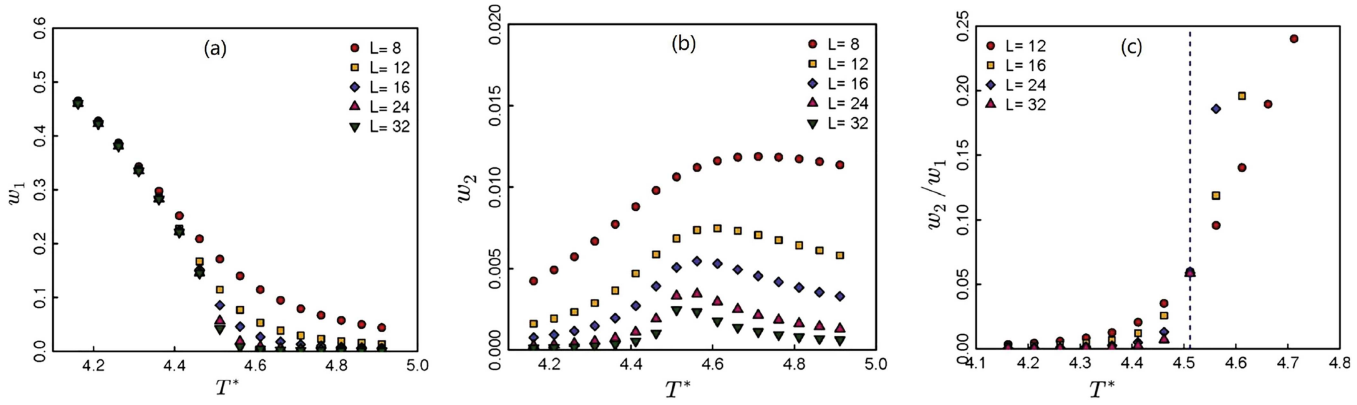


**FIG. 5.** (a) The weight $w_1$ corresponding to the largest eigen-ensemble matrix with respect to the dimensionless temperature $T^* = k_B T/J$ for system sizes $L = 8$, 12, 16, 24, and 32. (b) The weight $w_2$ with respect to the dimensionless temperature $T^*$ for different system sizes. (c) The ratio $w_2/w_1$ with respect to the dimensionless temperature $T^*$. Reproduced with permission from Hu *et al.*, Sci. China Phys. Mech. Astron. **62**, 990511 (2019). Copyright 2019 Science China Press.

dimensionless data as

$$\delta S_i(t) = \delta T_i(t)/\Delta_i, \tag{131}$$

which constitutes the elements of the microstate of the Earth $\delta \boldsymbol{S}_i(t)$.

In Fig. 6, we present the first six eigen-microstates $U_i$ with $i = 1, 2, \ldots, 6$ in the left columns of Figs. 6(a)–6(f), respectively. The evolutions of the corresponding eigen-microstates $V_i(t)$ are given in the right columns of Figs. 6(a)–6(f).

As presented in Fig. 6(a), EM1 reveals a classic solstitial mode and contributes 54.38% of the total variance. The spatial pattern exhibits an inter-hemisphere contrast. A robust one-year oscillation shown in 6(a) can be found, following the annual variation of the solar zenith angle.

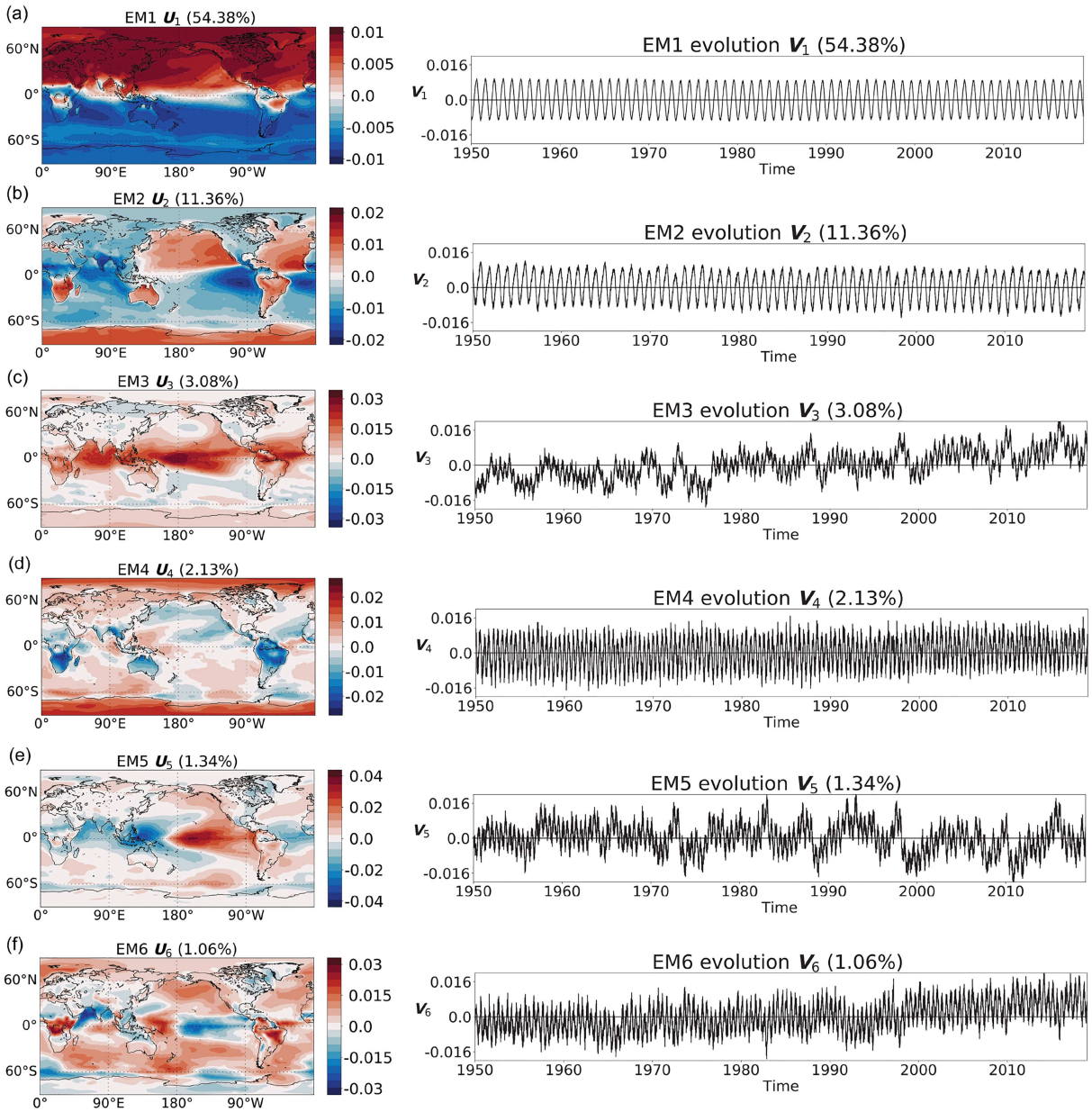


**FIG. 6.** (a)–(f) The evolution of the six largest eigen-microstates $V_i(t)$ of the Earth. The contributions of these states to the total variance are 54.38%, 11.36%, 3.08%, 2.13%, 1.34%, and 1.06%, respectively. Reproduced with permission from Sun *et al.*, Commun. Theor. Phys. **73**, 065603 (2021). Copyright 2021 Editorial Office of Communications in Theoretical Physics.

A remarkable land–sea contrast is observed in EM2 shown by Fig. 6(b), representing the land–sea contrasts of SAT, which is regarded as the primary driver for monsoon. The EM2 mode contributes to 11.36% of the total variance with also a one-year period oscillation implying the regular annual variation.

The eigenstate EM3 in Fig. 6(c) accounts for 3.08% of the total variance and is featured as the climate fluctuation within the tropics.

The eigenmode EM4 in Fig. 6(d) is a semiannual-oscillation (SAO) mode constituting 2.13% of the total variance, whose pattern is shown as significant temperature anomalies located in the tropics and high latitudes.

EM5 presented in Fig. 6(e) is a typical ENSO mode over the tropical Pacific Ocean accounting for 1.34% of the total variance. The warming over the central to eastern Pacific and cooling over the western Pacific is the strongest climate fluctuation at interannual time scale from 2 to 7 years.

The EM6 eigenmode in Fig. 6(f) reflects the well-known Indian Ocean Dipole mode and explains 1.06% of total variance.

The rest of the eigen-microstates occupy the proportions of the total variance less than 1%, and their spatial distributions vary in very small length scales.

### 3. Example 3: Price fluctuations in stock markets

As an example, let us consider the global stock market as a complex system and focus on the exploration of its principal fluctuation modes. Fluctuations of stock prices are consequences of complicated interactions of multiple factors in real life. The stock price is a direct indicator of the average expectation of an asset value asserted by all its investors. Due to limitations of information, an accurate judgment of stock prices is insufficient. Collective behaviors of investors can result in fluctuation patterns of stock prices. To some degree, these patterns reflect developments of related industries and companies. Here, we study the eigen-microstates of stock markets to analyze the fluctuation patterns of stock prices.

Suppose the price of a stock, say $i$, at a time $t$ is denoted by $P_i(t)$. The average price of stock $i$ during a specified period can be calculated as

$$\langle P_i(t)\rangle = \frac{1}{M}\sum_{t=1}^{N} P_i(t). \tag{132}$$

Here, $M$ refers to the total number of trading days. At time $t$, the $i$th stock has the price fluctuation $\delta P_i(t) = P_i(t) - \langle P_i(t)\rangle$, and the fluctuation is $\Delta_i = \sqrt{\frac{1}{M}\sum_{t=1}^{N}\delta P_i^2(t)}$. Then, the state of stock $i$ at time $t$ is characterized by the reduced fluctuation as $\delta S_i(t) = \delta P_i(t)/\Delta_i$. One finally obtains the microstate of the stock markets with $N$ stock prices described by the vector given in Eq. (107) with components $\delta S_i(t)$.

We take the stock price data from January 4, 2010 to May 26, 2020 in the Chinese mainland for investigations. The stock price data come from the public data published by Shanghai Stock Exchange (SSE) and Shenzhen Stock Exchange during the period from January 4, 2010 to May 26, 2020. In the dataset, there are 1600 stocks with prices of 2525 trading days. One adopts 1460 stocks for our analysis database by discarding the impaired data of 140 stocks.

For financial markets, composite indexes are constructed to describe their global trends. The SSE 100 Index reflects the performance of the entire Shanghai Stock Exchange market. It is composed of 100 sample stocks, which have rapid operating income growth and high return on equity in the market. The SSE sector indices reflect the performances of ten industry sectors: the energy sector, the materials sector, the industrials sector, etc. Two important indices of them are the SSE energy sector index and SSE materials sector index.

Based on the EMA scheme, the largest three eigen-microstates EM1 $U_1$, EM2 $U_2$, and EM3 $U_3$ are computed and shown in Fig. 7. Our numerical results indicate that eigen-microstates $U_1$, $U_2$, and $U_3$ occupy portions of 48.78%, 19.2%, and 8.54% of the total variance, respectively. The EM1 evolution $V_1$ is shown in Fig. 8(a) as the black line. Our result resembles the SSE100 Index perfectly well with a Pearson correlation $R = 0.95$. The evolution of EM2 $V_2$ and EM3 $V_3$ is shown in Figs. 8(b) and 8(c) as black lines, respectively. It can be found that these two lines are similar to the SSE energy sector and materials sector indices with Pearson correlations $R = 0.84$ and 0.75, respectively. These coincidences indicate that the eigen-fluctuation patterns in stock markets can be well captured by the eigen-microstates above.[21]

### 4. Example 4: Collective motion in living systems

The first application of the EMA to the non-equilibrium dynamics involves collective motions in living systems.[139]

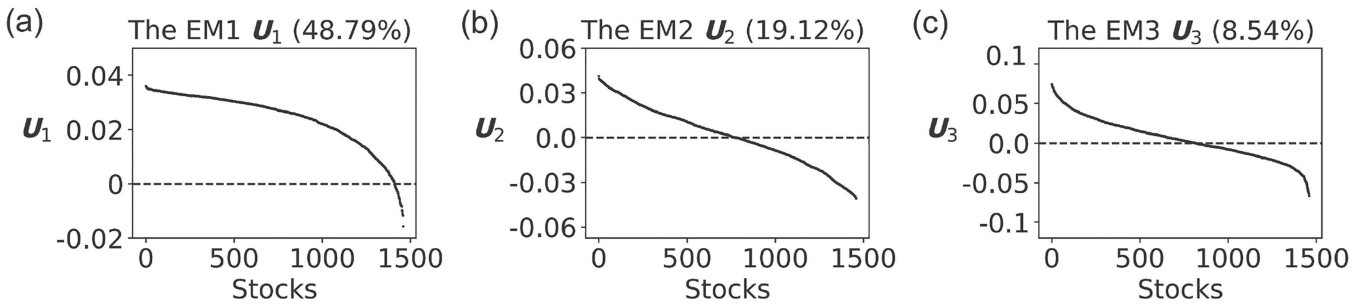


**FIG. 7.** (a)–(c) The largest three eigen-microstates $U_1$, $U_2$, and $U_3$ with respect to the stock system. Reproduced with permission from Sun *et al.*, Commun. Theor. Phys. **73**, 065603 (2021). Copyright 2021 Editorial Office of Communications in Theoretical Physics.

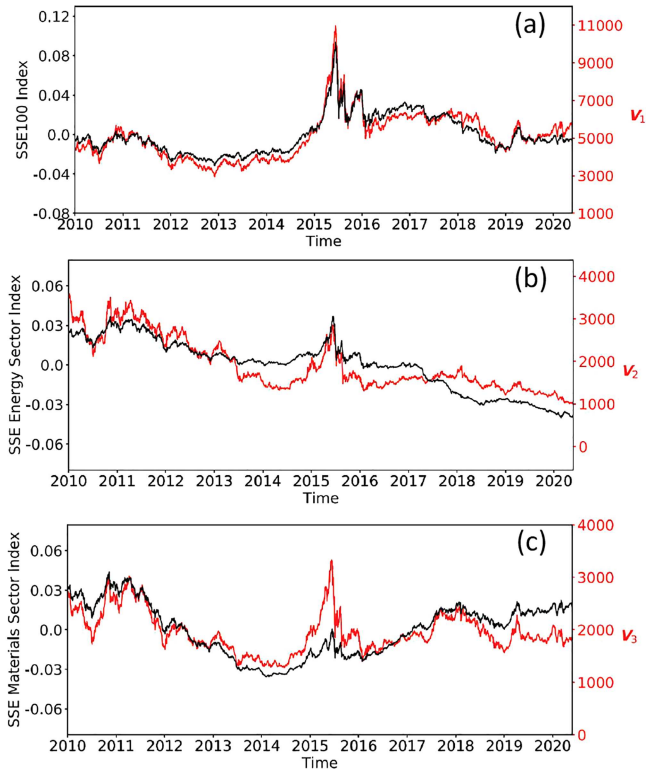


**FIG. 8.** (a) The evolutions of $V_1$ (red line) and the SSE100 index (black line). (b) The evolutions of $V_2$ (red line) and the SSE Energy Sector Index (black line). (c) The evolutions of $V_3$ (red line) and the SSE materials sector index (black line). Reproduced with permission from Sun *et al.*, Commun. Theor. Phys. **73**, 065603 (2021). Copyright 2021 Editorial Office of Communications in Theoretical Physics.

Collective motion of large groups of individuals has been ubiquitously observed in starlings,[140–142] bacterial communities,[143,144] ant colonies,[145] locusts,[146] midges,[147] and sheep.[148] It is significant to seek for universal features behind these seemingly diverse observations and the models sufficient to capture the fundamental features to find the fundamental principles of collective motion.

A prototype model of collective motion in living systems is the Vicsek model.[149] A two-dimensional Vicsek model is composed of $N = L \times L$ particles that are placed randomly on a two-dimensional domain with size $L$ and periodic boundary conditions. Particles move synchronously at discrete time steps by a fixed distance $v_0\Delta t$ with $v_0$ being the velocity. The time step $\Delta t = 1$. Each particle possesses with an aligning angle $\theta_i$ that determines the direction of the movement at the next time step. The angle is updated by the orientations of its neighbors through an averaged angle as

$$\langle\theta_i(t)\rangle_r = \Theta\left[\sum_{j:d_{ij}<1} \boldsymbol{v}_j(t)\right], \tag{133}$$

where $\Theta[\boldsymbol{v}]$ means the aligning angle of the vector $\boldsymbol{v}$ and $d_{ij}$ is the distance between particles $i$ and $j$. Then, the evolution of the Vicsek model can be written as

$$x_i(t+\Delta t) = x_i(t) + v_i(t+\Delta t)\Delta t, \tag{134}$$

$$\theta_i(t+\Delta t) = \langle\theta_i(t)\rangle_r + \eta\xi_i(t). \tag{135}$$

Here, the key ingredient is the competition between the tendency toward local alignment and the angular noise $\xi_i(t)$ that might come from external perturbations and/or from uncertainties in individuals perception, chosen from a uniform distribution within the interval $[-1/2, 1/2]$. The amplitude of noise $\eta$ has a maximum value $\eta_{\max} = 2\pi$. In the absence of noise, i.e., $\eta = 0$, all particles exhibit perfect alignment.

It was claimed that the phase transition of collective motion is continuous, but this was challenged later by Chaté *et al.*[150,151] They showed that the continuous nature observed is actually due to finite-size effects and the phase transition is discontinuous. Since the precise order parameter of collective motion is unknown and no systematic analysis of finite-size scaling has been made, these results about the nature.

We recently found a discontinuous transition of density and a continuous transition of velocity in the Vicsek models of collective motion, which are identified by the finite-size scaling form of order parameter. At strong noise, living systems behave like a gas. With the decrease of noise, the interactions between the particles of a living system become stronger and make them come closer. The living system experiences then a discontinuous gas–liquid-like transition of density. The even stronger interactions at smaller noise make the velocity directions of the particles become ordered and there is a continuous phase transition of collective motion in addition.

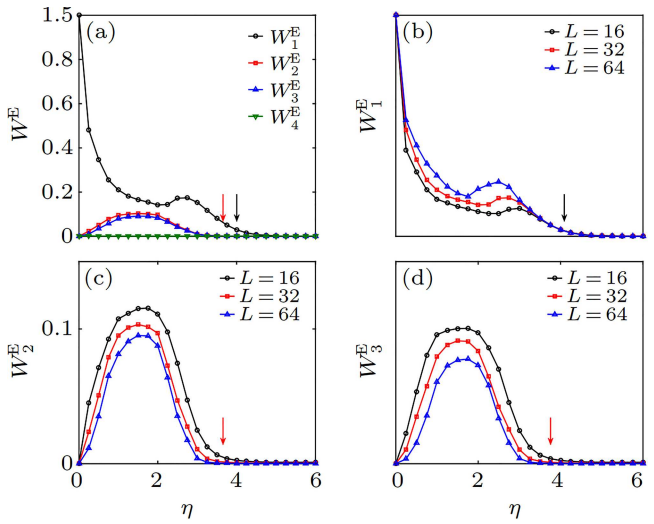


**FIG. 9.** The probabilities $W_l^E$ of the eigen-microstates in SVM with parameters $\rho = 2$ and $v_0 = 0.5$. (a) $W_l^E$ at L = 32. (b)–(d) $W_1^E$, $W_2^E$, and $W_3^E$ at different sizes, respectively. Reproduced with permission from Li *et al.*, Chin. Phys. B **30**, 128703 (2021). Copyright 2021 Editorial Office of Chinese Physics B.

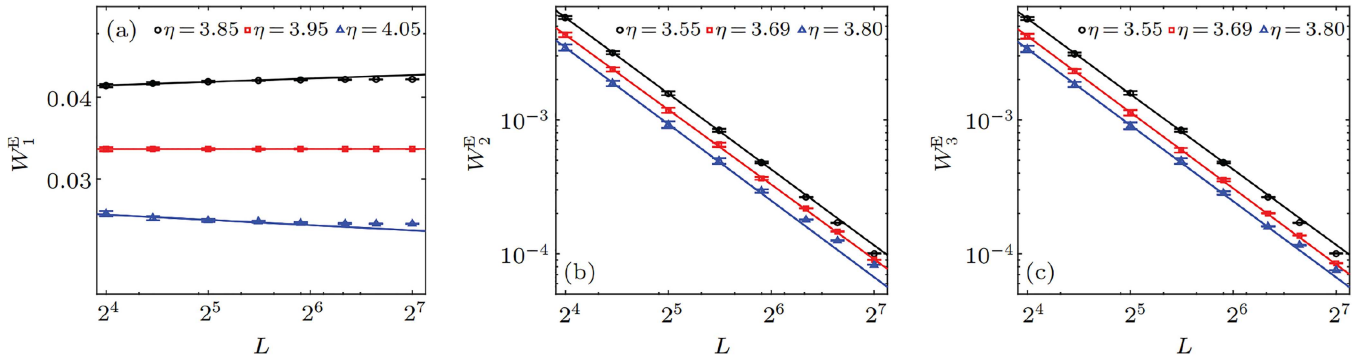


**FIG. 10.** log $W_I^E$ vs log $L$ around phase transition points. (a) $\eta_{1c} = 3.95$ and $\beta_1/\nu_1 = 0.0000(5)$. (b) $\eta_{2c} = 3.69$ and $\beta_2/\nu_2 = 0.94(1)$. (c) $\eta_{3c} = 3.69$ and $\beta_3/\nu_3 = 0.94(2)$. Reproduced with permission from Li *et al.*, Chin. Phys. B **30**, 128703 (2021). Copyright 2021 Editorial Office of Chinese Physics B.

Figure 9 shows the relationship between the weights of the main eigen-microstates and the noise strength. It can be seen from Fig. 9(a) that as the noise decreases, the $W_1^E$ mode condenses first, and then the $W_2^E$ mode and $W_3^E$ mode condense simultaneously. Figures 9(a), 9(c), and 9(d) demonstrate the size effect of $W_1^E$, $W_2^E$, and $W_3^E$. Accurate critical point calculations require resorting to finite-size scaling analysis. In the critical regime, the eigen-microstate weights should satisfy the finite-size scaling relationship

$$W_I^{\mathrm{E}}(\eta, L) = L^{-2\beta/\nu} \tilde{W}_I^{\mathrm{E}}\left(hL^{1/\nu}\right), \tag{136}$$

where $\tilde{W}_I^{\mathrm{E}}$ is a universal scaling function, $\beta$ is the critical exponent of the order parameter, and $\nu$ is the critical exponent of the correlation length. Taking logarithm to both sides of Eq. (136), one obtains

$$\ln W_I^{\mathrm{E}}(\eta, L) = -2\beta/\nu \ln L + \ln \tilde{W}_I^{\mathrm{E}}\left(hL^{1/\nu}\right). \tag{137}$$

From this formula, we can clearly see that the relationship between $\ln \tilde{W}_I^{\mathrm{E}}$ and $\ln L$ satisfies a perfect linear relationship only at the critical point. Its slope reveals the ratio of critical exponents.

Figure 10 shows the log–log relationship between the eigen-microstate weights and system sizes. It can be concluded that there are two different phase transitions in the standard Vicsek model (SVM). The first phase transition corresponds to the emergency of the $W_1^E$ mode at $\eta = 3.95$. Its critical exponent is $\beta/\nu = 0$, which means that this is a discontinuous phase transition. The second phase transition corresponds to the condensation of $W_2^E$ and $W_2^E$ at $\eta = 3.69$. Its critical exponent takes a finite value, implying that this is a continuous phase transition.

## VII. CONCLUDING REMARKS AND PERSPECTIVES

Collective dynamics in complex systems implies the emergence of order from complexity. Order parameters in describing the orderness are embedded in the dynamics and may spontaneously emerge rather than be manually selected. In this review, we extensively discussed the order-parameter dynamics of complex systems. By applying the slaving principle in disclosing the competitions among various state variables with different time scales, it is shown that at the critical point, only a few slow-varying modes eventually conquer a large number of fast modes and dominate the evolution of the system. These slow modes grow up from a large number of degrees of freedom and act as order parameters. The evolution of these small number of order parameters well represents the collective dynamics and is a great dimension reduction of complex systems.

It should be stressed that the idea of the reduction scheme can be extensively applied to various macroscopic collective transitions in complex systems, such as the emergence of spatiotemporal patterns, the transitions from partial to global synchronization in coupled oscillators, the transitions from non-integrability to integrability in Hamiltonian systems, thermodynamic phase transitions in condensed matters, and so on. Slaving principle and more generally the principles in synergetic theory and dissipative-structure theory are exhibiting their great privileges in exploring the order emergence of complex systems in recent years.

An effective reduction can often be highlighted from some intrinsic physical properties of complex systems. For example, symmetry is a well-known solvable case in physics, which mathematically corresponds to certain transformation invariance. For example, symmetries in a Hamiltonian system lead to various invariant integrals and constants of motion, which naturally limit the motion in a lower-dimensional space. If the number of independent constants equals the degree of freedom, the motion of the system is integrable. Another example is hydrodynamics, where the microscopic collision invariances (conservation laws) lead to the reduction to the Boltzmann equation and the Navier–Stokes equation.

The slaving principle we discussed in this paper is closely related to the separation of time scales of different degrees of freedom. This reminds us of the emergence of order at the onset of phase transition in statistical physics, at which the slowing down effect can be observed and only a few stable modes become unstable and dominate the global behavior of the system. Physically, the relaxation time scale is related to the correlation time scale, and the spatial diffusion scale is related to the spatial correlation scale. A large distinction of time or space scales naturally leads to the separation of state variables. An impressive example is the theoretical foundation of Brownian motion. The Langevin equation is a stochastic equation of motion including both deterministic and random forces due to the time-scale separation of the relaxational time

and the rapid thermal fluctuation. Statistical dynamics of Brownian-related processes distributed from physics to chemistry and biology becomes an important subject.

In this minireview, we extensively discussed theoretical descriptions and explorations of the collective dynamics of complex systems from the viewpoint of order-parameter dynamics. We adopt the slaving principle as the foundation of order-parameter theory in reducing the complicated dynamics of systems with multiple degrees of freedom. As a prototype practice, the synchronization of coupled phase oscillators is analytically studied, and the order-parameter dynamics is studied in terms of the Ott–Antonsen ansatz. This idea is also applied to the exploration of neuron dynamics. Practically, the order-parameter dynamics can also be accomplished for the spatiotemporal data obtained from complex systems by introducing the eigen-microstate approach.

Extensive studies have been made very recently[11,152–161] on the collective dynamics of swarmalator systems, also called swarming oscillators, i.e., oscillators whose phase dynamics and spatially swarming dynamics are mutually coupled. This topic was first experimentally discussed in relating to the pattern formation and traveling waves in myxobacteria[162] and then was theoretically proposed by Tanaka.[163] This is a natural merging between spatial swarming dynamics and intrinsic synchronization dynamics, order-parameter dynamics plays a very important role in revealing many interesting spatiotemporal self-organization behaviors. On the one hand, theoretical studies can be applied as long as one is able to make a simplification on modeling of these systems. On the other hand, one may adopt the eigen-microstate approach to investigate the collective dynamics of general swarmalator systems in reality by collecting and analyzing dynamic data and picking up spatiotemporal eigenmodes.

## ACKNOWLEDGMENTS

The authors thank the invitation from Professor Jurgen Kurths for this review. This work was partially supported by the National Natural Science Foundation of China (NNSFC) [Nos. 12375031 and 11875135 (Zheng); No. 11905068 (Xu); and Nos. 12275020 and 12135003 (Fan and Chen)].

## AUTHOR DECLARATIONS

### Conflict of Interest

The authors have no conflicts to disclose.

### Author Contributions

**Zhigang Zheng:** Conceptualization (equal); Data curation (equal); Formal analysis (equal); Funding acquisition (equal); Investigation (equal); Methodology (equal); Project administration (equal); Resources (equal); Software (equal); Supervision (equal); Validation (equal); Visualization (equal); Writing – original draft (equal); Writing – review & editing (equal). **Can Xu:** Data curation (equal); Funding acquisition (equal); Investigation (equal); Writing – original draft (equal). **Jingfang Fan:** Conceptualization (equal); Data curation (equal); Funding acquisition (equal); Investigation (equal); Methodology (equal); Resources (equal); Validation (equal); Visualization (equal); Writing – original draft (equal). **Maoxin Liu:** Data curation (equal); Formal analysis (equal); Investigation (equal); Visualization (equal); Writing – original draft (equal); Writing – review & editing (equal). **Xiaosong Chen:** Conceptualization (equal); Data curation (equal); Formal analysis (equal); Funding acquisition (equal); Investigation (equal); Methodology (equal); Project administration (equal); Resources (equal); Software (equal); Supervision (equal); Validation (equal); Visualization (equal); Writing – original draft (equal); Writing – review & editing (equal).

## DATA AVAILABILITY

The data that support the findings of this study are available from the corresponding author upon reasonable request.

## REFERENCES

[1] Y. Kuramoto, *Chemical Oscillations, Waves, and Turbulence* (Springer-Verlag, 1984).
[2] Z. Zheng, *An Introduction to Emergence Dynamics in Complex Systems* (Springer Singapore, Singapore, 2021).
[3] M. E. Fisher, Rev. Mod. Phys. **70**, 653 (1998).
[4] H. Haken, *Advanced Synergetics: Instability Hierarchies of Self-Organizing Systems and Devices* (Springer, Berlin, 1983).
[5] A. T. Winfree, J. Theor. Biol. **16**, 15 (1967).
[6] E. Ott and T. M. Antonsen, Chaos **18**, 037113 (2008).
[7] E. Ott and T. M. Antonsen, Chaos **19**, 023117 (2009).
[8] F. Parastesh, S. Jafari, H. Azarnoush, Z. Shahriari, Z. Wang, S. Boccaletti, and M. Perc, Phys. Rep. **898**, 1 (2021).
[9] E. Montbrió, D. Pazó, and A. Roxin, Phys. Rev. X **5**, 021028 (2015).
[10] C. Bechinger, R. Di Leonardo, H. Löwen, C. Reichhardt, G. Volpe, and G. Volpe, Rev. Mod. Phys. **88**, 045006 (2016).
[11] K. P. O'Keeffe, H. Hong, and S. H. Strogatz, Nat. Commun. **8**, 1504 (2017).
[12] M. I. Rabinovich, P. Varona, A. I. Selverston, and H. D. I. Abarbanel, Rev. Mod. Phys. **78**, 1213 (2006).
[13] V. A. Huynh-Thu and G. Sanguinetti, *Gene Regulatory Network Inference: An Introductory Survey* (Springer New York, New York, NY, 2019).
[14] D. Sornette, Rep. Prog. Phys. **77**, 062001 (2014).
[15] S. Boccaletti, V. Latora, Y. Moreno, M. Chavez, and D.-U. Hwang, Phys. Rep. **424**, 175 (2006).
[16] J. Ren, W.-X. Wang, B. Li, and Y.-C. Lai, Phys. Rev. Lett. **104**, 058701 (2010).
[17] P. Yang, Q. Wang, and Z. Zheng, Phys. Rev. E **86**, 026203 (2012).
[18] Z. Zhang, Z. Li, G. Hu, and Z. Zheng, Europhys. Lett. **105**, 18003 (2014).
[19] H. Wang, C. Ma, H.-S. Chen, Y.-C. Lai, and H. Zhang, Nat. Commun. **13**, 3043 (2022).
[20] Z. Yan, L.-X. Gui, K. Xu, and Y. Lan, New J. Phys. **25**, 083011 (2023).
[21] Y. Sun, G. Hu, Y. Zhang, B. Lu, Z. Lu, J. Fan, X. Li, Q. Deng, and X. Chen, Commun. Theor. Phys. **73**, 065603 (2021).
[22] M. C. Cross and P. Hohenberg, Rev. Mod. Phys. **65**, 851 (1993).
[23] I. S. Aranson and L. Kramer, Rev. Mod. Phys. **74**, 99 (2001).
[24] M. Cross and H. Greenside, *Pattern Formation and Dynamics in Nonequilibrium Systems* (Cambridge University Press, 2009).
[25] V. García-Morales and K. Krischer, Contemp. Phys. **53**, 79 (2012).
[26] A. Pikovsky, M. Rosenblum, and J. Kurths, *Synchronization: A Universal Concept in Nonlinear Sciences* (Cambridge University Press, Cambridge, 2001).
[27] Z. Zheng, G. Hu, and B. Hu, Phys. Rev. Lett. **81**, 5318 (1998).
[28] Z. Zheng, B. Hu, and G. Hu, Phys. Rev. E **62**, 402 (2000).
[29] B. Hu and Z. Zheng, Int. J. Bifurcation Chaos **10**, 2399 (2000).
[30] J. Gao, C. Xu, Y. Sun, and Z. Zheng, Sci. Rep. **6**, 30184 (2015).
[31] H. Chen, Y. Sun, J. Gao, C. Xu, and Z. Zheng, Front. Phys. **12**, 120504 (2017).
[32] S. H. Strogatz and R. Mirollo, J. Stat. Phys. **63**, 613 (1991).

[33]R. Mirollo and S. H. Strogatz, Physica D **205**, 249 (2005).
[34]S. Watanabe and S. H. Strogatz, Phys. Rev. Lett. **70**, 2391 (1993).
[35]S. Watanabe and S. H. Strogatz, Physica D **74**, 197 (1994).
[36]S. A. Marvel, R. Mirollo, and S. H. Strogatz, Chaos **19**, 043104 (2009).
[37]S. A. Marvel and S. H. Strogatz, Chaos **19**, 013132 (2009).
[38]G. A. Gottwald, Chaos **25**, 053111 (2015).
[39]E. J. Hancock and G. A. Gottwald, Phys. Rev. E **98**, 012307 (2018).
[40]J. Fialkowski, S. Yanchuk, I. M. Sokolov, E. Schöll, G. A. Gottwald, and R. Berner, Phys. Rev. Lett. **130**, 067402 (2023).
[41]R. Cestnik and A. Pikovsky, Phys. Rev. Lett. **128**, 054101 (2022).
[42]J. A. Acebrón, L. L. Bonilla, C. J. P. Vicente, F. Ritort, and R. Spigler, Rev. Mod. Phys. **77**, 137 (2005).
[43]F. A. Rodrigues, T. K. D. M. Peron, P. Ji, and J. Kurths, Phys. Rep. **610**, 1 (2016).
[44]H. Hong and S. H. Strogatz, Phys. Rev. Lett. **106**, 054102 (2011).
[45]J. Park and B. Kahng, Physica D **399**, 186 (2019).
[46]C. Xu, S. Boccaletti, Z. Zheng, and S. Guan, New J. Phys. **21**, 113018 (2019).
[47]T. Qiu, S. Boccaletti, Z. Liu, and S. Guan, Phys. Rev. E **100**, 052310 (2019).
[48]E. Teichmann and M. Rosenblum, Chaos **29**, 093124 (2019).
[49]S. N. Chowdhury, D. Ghosh, and C. Hens, Phys. Rev. E **101**, 022310 (2020).
[50]T. Peron, Phys. Rev. E **103**, 042210 (2021).
[51]A. Sharma, Chaos Soliton. Fract. **145**, 110815 (2021).
[52]K. L. Kreienkamp and S. H. L. Klapp, New J. Phys. **24**, 123009 (2022).
[53]M. Manoranjani, D. Senthilkumar, and V. Chandrasekar, Chaos Soliton. Fract. **167**, 113018 (2023).
[54]T. Tanaka and T. Aoyagi, Phys. Rev. Lett. **106**, 224101 (2011).
[55]P. S. Skardal, E. Ott, and J. G. Restrepo, Phys. Rev. E **84**, 036208 (2011).
[56]M. Komarov and A. Pikovsky, Phys. Rev. E **92**, 020901 (2015).
[57]C. Xu, Y. Sun, J. Gao, T. Qiu, Z. Zheng, and S. Guan, Sci. Rep. **6**, 21926 (2016).
[58]P. S. Skardal and A. Arenas, Phys. Rev. Lett. **122**, 248301 (2019).
[59]X. Wang, Z. Zheng, and C. Xu, Phys. Rev. E **104**, 054208 (2021).
[60]X. Wang, C. Xu, and Z. Zheng, Nonlinear Dyn. **103**, 2721 (2021).
[61]H. Wang and X. Li, Phys. Rev. E **83**, 066214 (2011).
[62]J. Gómez-Gardeñes, S. Gómez, A. Arenas, and Y. Moreno, Phys. Rev. Lett. **106**, 128701 (2011).
[63]X. Zhang, X. Hu, J. Kurths, and Z. Liu, Phys. Rev. E **88**, 010802 (2013).
[64]R. S. Pinto and A. Saa, Phys. Rev. E **91**, 022818 (2014).
[65]S. Boccaletti, J. Almendral, S. Guan, I. Leyva, Z. Liu, I. Sendia-Nadal, Z. Wang, and Y. Zou, Phys. Rep. **660**, 1 (2016).
[66]R. M. D'Souza, J. G'omez-Gardenes, J. Nagler, and A. Arenas, Adv. Phys. **68**, 123 (2019).
[67]W. Zou and J. Wang, Phys. Rev. E **102**, 012219 (2020).
[68]Y. Wu, Z. Zheng, L. Tang, and C. Xu, Chaos Soliton. Fract. **164**, 112680 (2022).
[69]F. Ritort, Phys. Rev. Lett. **80**, 6 (1998).
[70]C. Zheng, R. Toenjes, and A. Pikovsky, Phys. Rev. E **104**, 014216 (2021).
[71]J. Zhu, Phys. Lett. A **377**, 2939 (2013).
[72]T. Tanaka, New J. Phys. **16**, 023016 (2014).
[73]S. Chandra, M. Girvan, and E. Ott, Phys. Rev. X **9**, 011002 (2019).
[74]S. Chandra, M. Girvan, and E. Ott, Chaos **29**, 053107 (2019).
[75]S. Chandra and E. Ott, Chaos **29**, 033124 (2019).
[76]M. Lipton, R. Mirollo, and S. H. Strogatz, Chaos **31**, 093113 (2019).
[77]X. Dai, X. Li, H. Guo, D. Jia, M. Perc, P. Manshour, Z. Wang, and S. Boccaletti, Phys. Rev. Lett. **125**, 194101 (2020).
[78]W. Zou, S. He, D. V. Senthilkumar, and J. Kurths, Phys. Rev. Lett. **130**, 107202 (2023).
[79]K. Kovalenko, X. Dai, K. Alfaro-Bittner, A. M. Raigorodskii, M. Perc, and S. Boccaletti, Phys. Rev. Lett. **127**, 258301 (2021).
[80]B. Ermentrout, J. Math. Biol. **29**, 571 (1991).
[81]D. Witthaut, F. Hellmann, J. Kurths, S. Kettemann, H. Meyer-Ortmanns, and M. Timme, Rev. Mod. Phys. **94**, 015005 (2022).
[82]G. Filatrella, A. H. Nielsen, and N. F. Pedersen, Eur. Phys. J. B **61**, 485 (2008).
[83]P. J. Menck, J. Heitzig, N. Marwan, and J. Kurths, Nat. Phys. **9**, 89 (2013).
[84]P. Ji, T. K. D. Peron, F. A. Rodrigues, and J. Kurths, Phys. Rev. E **90**, 062810 (2014).
[85]P. Ji, W. Lu, and J. Kurths, Europhys. Lett. **122**, 40003 (2018).
[86]P. J. Menck, J. Heitzig, J. Kurths, and H. Joachim Schellnhuber, Nat. Commun. **5**, 1 (2014).
[87]M. Brede, Phys. Lett. A **372**, 2618 (2008).
[88]P. S. Skardal, D. Taylor, and J. Sun, Phys. Rev. Lett. **113**, 144101 (2014).
[89]X. Li, W. Wei, and Z. Zheng, Chaos **33**, 063149 (2023).
[90]H.-A. Tanaka, A. J. Lichtenberg, and S. Oishi, Phys. Rev. Lett. **78**, 2104 (1997).
[91]J. Gao and K. Efstathiou, Phys. Rev. E **98**, 042201 (2018).
[92]J. Gao and K. Efstathiou, Chaos **31**, 093137 (2021).
[93]G. Csaba and W. Porod, Appl. Phys. Rev. **7**, 011302 (2020).
[94]Y. Zhang, Y. Deng, Y. Lin, Y. Jiang, Y. Dong, X. Chen, G. Wang, D. Shang, Q. Wang, H. Yu *et al.*, Micromachines **13**, 1016 (2022).
[95]T. Wang and J. S. Roychowdhury, in International Conference on Unconventional Computation and Natural Computation (Springer Nature, 2019), pp. 232–256; see arXiv:1903.07163.
[96]T. Wang, L. Wu, P. Nobel, and J. S. Roychowdhury, Nat. Comput. **20**, 287 (2021).
[97]A. Houshang, M. Zahedinejad, S. Muralidhar, J. Checiński, R. Khymyn, M. Rajabali, H. Fulara, A. A. Awad, M. Dvornik, and J. Åkerman, Phys. Rev. Appl. **17**, 014003 (2022).
[98]A. Grimaldi, L. Mazza, E. Raimondo, P. Tullo, D. Rodrigues, K. Y. Camsari, V. Crupi, M. Carpentieri, V. Puliafito, and G. Finocchio, Phys. Rev. Appl. **20**, 024005 (2023).
[99]A. Kumar, H. Fulara, R. Khymyn, A. Litvinenko, M. Zahedinejad, M. Rajabali, X. Zhao, N. Behera, A. Houshang, A. A. Awad *et al.*, Nano Lett. **23**, 6720 (2023).
[100]J. Chou, S. Bramhavar, S. Ghosh, and W. Herzog, Sci. Rep. **9**, 14786 (2019).
[101]Y. Kuramoto and D. Battogtokh, Nonlinear Phenom. Complex Syst. **5**, 380 (2002), http://www.j-npcs.org/abstracts/vol2002/v5no4/v5no4p380.html.
[102]D. M. Abrams and S. H. Strogatz, Phys. Rev. Lett. **93**, 174102 (2004).
[103]D. M. Abrams and S. H. Strogatz, Int. J. Bifurcation Chaos **16**, 21 (2006).
[104]O. E. Omel'chenko, M. Wolfrum, and Y. L. Maistrenko, Phys. Rev. E **81**, 065201 (2010).
[105]M. Wolfrum and O. E. Omel'chenko, Phys. Rev. E **84**, 015201 (2011).
[106]D. M. Abrams, R. Mirollo, S. H. Strogatz, and D. A. Wiley, Phys. Rev. Lett. **101**, 084103 (2008).
[107]C. R. Laing, Physica D **238**, 1569 (2009).
[108]O. E. Omel'chenko, Nonlinearity **26**, 2469 (2013).
[109]I. Omelchenko, Y. L. Maistrenko, P. Hövel, and E. Schöll, Phys. Rev. Lett. **106**, 234102 (2011).
[110]I. Omelchenko, B. Riemenschneider, P. Hövel, Y. L. Maistrenko, and E. Schöll, Phys. Rev. E **85**, 026212 (2012).
[111]B. K. Bera, D. Ghosh, and M. Lakshmanan, Phys. Rev. E **93**, 012205 (2016).
[112]I. A. Shepelev, T. E. Vadivasova, G. I. Strelkova, and V. S. Anishchenko, Phys. Lett. A **381**, 1398 (2017).
[113]E. A. Martens, C. R. Laing, and S. H. Strogatz, Phys. Rev. Lett. **104**, 044101 (2010).
[114]S. R. Ujjwal and R. Ramaswamy, Phys. Rev. E **88**, 032902 (2013).
[115]A. S. Zakharova, M. L. Kapeller, and E. Schöll, Phys. Rev. Lett. **112**, 154101 (2014).
[116]U. K. Verma and G. Ambika, Chaos **30**, 043104 (2020).
[117]G. G. Mascetti, Nature Sci. Sleep **8**, 221 (2016).
[118]M. Tamaki, J. W. Bang, T. Watanabe, and Y. Sasaki, Curr. Biol. **26**, 1190 (2016).
[119]M. Gerster, R. Berner, J. Sawicki, A. S. Zakharova, A. Škoch, J. Hlinka, K. Lehnertz, and E. Schöll, Chaos **30**, 123130 (2020).
[120]E. M. Izhikevich, *Dynamical Systems in Neuroscience: The Geometry of Excitability and Bursting* (MIT Press, Cambridge, MA, 2006).
[121]G. Hahn, A. Ponce-Alvarez, G. Deco, A. Aertsen, and A. Kumar, Nat. Rev. Neurosci. **20**, 117 (2018).
[122]B. B. Averbeck, P. E. Latham, and A. Pouget, Nat. Rev. Neurosci. **7**, 358 (2006).
[123]R. Brette, M. Rudolph-Lilith, N. T. Carnevale, M. L. Hines, D. Beeman, J. M. Bower, M. Diesmann, A. Morrison, P. H. Goodman, F. C. Harris *et al.*, J. Comp. Neuron. **23**, 349 (2007).
[124]M. Lundqvist, J. Rose, P. A. Herman, S. L. Brincat, T. J. Buschman, and E. K. Miller, Neuron **90**, 152 (2016).
[125]W. Gerstner and W. M. Kistler, *Spiking Neuron Models: Single Neurons, Populations, Plasticity* (Cambridge University Press, Cambridge, 2002).
[126]G. B. Ermentrout and D. H. Terman, *Mathematical Foundations of Neuroscience* (Springer, New York, 2010), Vol. 64.

[127]I. Ratas and K. Pyragas, Phys. Rev. E **94**, 032215 (2016).
[128]I. Ratas and K. Pyragas, Phys. Rev. E **100**, 052211 (2019).
[129]D. Pazó and E. Montbrió, Phys. Rev. Lett. **116**, 238101 (2016).
[130]F. Devalle, E. Montbrió, and D. Pazó, Phys. Rev. E **98**, 042214 (2018).
[131]K. Pyragas, A. P. Fedaravivcius, and T. Pyragiene, Phys. Rev. E **104**, 014203 (2021).
[132]H. Bi, M. di Volo, and A. Torcini, Front. Syst. Neurosci. **15**, 752261 (2021).
[133]E. Montbri'o and D. Paz'o, Phys. Rev. Lett. **125**, 248101 (2020).
[134]D. S. Goldobin, M. di Volo, and A. Torcini, Phys. Rev. Lett. **127**, 038301 (2021).
[135]G. Hu, T. Liu, M. Liu, W. Chen, and X. Chen, Sci. China Phys. Mech. Astron. **62**, 990511 (2019).
[136]V. Lucarini, R. Blender, C. Herbert, F. Ragone, S. Pascale, and J. Wouters, Rev. Geophys. **52**, 809 (2014).
[137]J. Fan, J. Meng, J. Ludescher, X. Chen, Y. Ashkenazy, J. Kurths, S. Havlin, and H. J. Schellnhuber, Phys. Rep. **896**, 1 (2021).
[138]E. Kalnay, M. Kanamitsu, R. Kistler, W. Collins, D. Deaven, L. Gandin, M. Iredell, S. Saha, G. White, J. Woollen *et al.*, Bull. Am. Meteorol. Soc. **77**, 437 (1996).
[139]X. Li, T. Xue, Y. Sun, J. Fan, H. Li, M. Liu, Z. Han, Z. Di, and X. Chen, Chin. Phys. B **30**, 128703 (2021).
[140]A. Cavagna, A. Cimarelli, I. Giardina, G. Parisi, R. Santagati, F. Stefanini, and M. Viale, Proc. Natl. Acad. Sci. U.S.A. **107**, 11865 (2009).
[141]W. Bialek, A. Cavagna, I. Giardina, T. Mora, E. Silvestri, M. Viale, and A. M. Walczak, Proc. Natl. Acad. Sci. U.S.A. **109**, 4786 (2011).
[142]W. Bialek, A. Cavagna, I. Giardina, T. Mora, O. Pohl, E. Silvestri, M. Viale, and A. M. Walczak, Proc. Natl. Acad. Sci. U.S.A. **111**, 7212 (2013).
[143]X. Chen, X. Dong, A. Be'er, H. L. Swinney, and H. P. Zhang, Phys. Rev. Lett. **108**, 148101 (2012).
[144]H. Li, X. qing Shi, M. Huang, X. Chen, M. Xiao, C. Liu, H. Chaté, and H. P. Zhang, Proc. Natl. Acad. Sci. U.S.A. **116**, 777 (2018).
[145]O. Feinerman, I. Pinkoviezky, A. Gelblum, E. Fonio, and N. S. Gov, Nat. Phys. **14**, 683 (2018).
[146]J. Buhl, D. J. T. Sumpter, I. D. Couzin, J. J. Hale, E. Despland, E. R. Miller, and S. J. Simpson, Science **312**, 1402 (2006).
[147]A. Attanasi, A. Cavagna, L. D. Castello, I. Giardina, S. Melillo, L. Parisi, O. Pohl, B. Rossaro, E. Shen, E. Silvestri *et al.*, Phys. Rev. Lett. **113**, 238102 (2014).
[148]F. Ginelli, F. Peruani, M.-H. Pillot, H. Chaté, G. Theraulaz, and R. Bon, Proc. Natl. Acad. Sci. U.S.A. **112**, 12729 (2015).
[149]T. Vicsek, A. Czirók, E. Ben-Jacob, I. Cohen, and O. Shochet, Phys. Rev. Lett. **75**, 1226 (1995).
[150]G. Grégoire and H. Chaté, Phys. Rev. Lett. **92**, 025702 (2004).
[151]H. Chaté, F. Ginelli, G. Grégoire, and F. Raynaud, Phys. Rev. E **77**, 046113 (2008).
[152]H. Hong, Chaos **28**, 103112 (2018).
[153]K. P. O'Keeffe, J. H. M. Evers, and T. Kolokolnikov, Phys. Rev. E **98**, 022203 (2018).
[154]F. Jiménez-Morales, Phys. Rev. E **101**, 062202 (2020).
[155]T. A. McLennan-Smith, D. O. Roberts, and H. S. Sidhu, Phys. Rev. E **102**, 032607 (2020).
[156]M. Fruchart, R. Hanai, P. B. Littlewood, and V. Vitelli, Nature **592**, 363 (2021).
[157]H. Hong, K. Yeo, and H. K. Lee, Phys. Rev. E **104**, 044214 (2021).
[158]H. K. Lee, K. Yeo, and H. Hong, Chaos **31**, 033134 (2021).
[159]K. O'Keeffe, S. Ceron, and K. Petersen, Phys. Rev. E **105**, 014211 (2022).
[160]G. K. Sar, S. N. Chowdhury, M. Perc, and D. Ghosh, New J. Phys. **24**, 043004 (2022).
[161]S. Yoon, K. P. O'Keeffe, J. F. F. Mendes, and A. V. Goltsev, Phys. Rev. Lett. **129**, 208002 (2022).
[162]O. A. Igoshin, A. Mogilner, R. D. Welch, D. Kaiser, and G. F. Oster, Proc. Natl. Acad. Sci. U.S.A. **98**, 14913 (2001).
[163]D. Tanaka, Phys. Rev. Lett. **99**, 134103 (2007).
[164]N. Yao, and Z. G. Zheng, Int. J. Mod. Phys. B **30**, 1630002 (2016).